HHS Public Access

Author manuscript

Neurobiol Dis. Author manuscript; available in PMC 2018 April 01.

Published in final edited form as:

Neurobiol Dis. 2018 April ; 112: 63–78. doi:10.1016/j.nbd.2018.01.007.

Glial scars are permeable to the neurotoxic environment of chronic stroke infarcts

Jacob C. Zbesko[a], **Thuy-Vi V. Nguyen**[a,b], **Tao Yang**[e], **Jennifer Beischel Frye**[a], **Omar Hussain**[a], **Megan Hayes**[a], **Amanda Chung**[a], **W. Anthony Day**[d], **Kristina Stepanovic**[a], **Maj Krumberger**[a], **Justine Mona**[a], **Frank M. Longo**[e], **Kristian P. Doyle**[a,b,c,*]

[a]Department of Immunobiology, University of Arizona, Tucson, AZ 85719, USA

[b]Department of Neurology, University of Arizona, Tucson, AZ 85719, USA

[c]Arizona Center on Aging, University of Arizona, Tucson, AZ 85719, USA

[d]Arizona Health Sciences Center Imaging Core Facility, Arizona Research Labs, University of Arizona, Tucson, AZ 85719, USA

[e]Department of Neurology and Neurological Sciences, Stanford University School of Medicine, Stanford, CA 94305, USA

Abstract

Following stroke, the damaged tissue undergoes liquefactive necrosis, a stage of infarct resolution that lasts for months although the exact length of time is currently unknown. One method of repair involves reactive astrocytes and microglia forming a glial scar to compartmentalize the area of liquefactive necrosis from the rest of the brain. The formation of the glial scar is a critical component of the healing response to stroke, as well as other central nervous system (CNS) injuries. The goal of this study was to evaluate the toxicity of the extracellular fluid present in areas of liquefactive necrosis and determine how effectively it is segregated from the remainder of the brain. To accomplish this goal, we used a mouse model of stroke in conjunction with an extracellular fluid toxicity assay, fluorescent and electron microscopy, immunostaining, tracer injections into the infarct, and multiplex immunoassays. We confirmed that the extracellular fluid present in areas of liquefactive necrosis following stroke is toxic to primary cortical and hippocampal neurons for at least 7 weeks following stroke, and discovered that although glial scars are robust physical and endocytic barriers, they are nevertheless permeable. We found that molecules present in the area of liquefactive necrosis can leak across the glial scar and are removed by a combination of paravascular clearance and microglial endocytosis in the adjacent tissue. Despite these mechanisms, there is delayed atrophy, cytotoxic edema, and neuron loss

*Corresponding author at: Department of Immunobiology, University of Arizona, Tucson, 1656 E. Mabel Street, Tucson, AZ 85719, USA. doylekr@email.arizona.edu (K.P. Doyle).

Ethical approval

All applicable international, national, and/or institutional guidelines for the care and use of animals were followed. As such, all experiments were conducted in accordance with protocols approved by the Animal Care and Use Committee of the University of Arizona and were performed based on the NIH Guide for the Care and Use of Laboratory Animals.

Conflict of interest

The authors declare that they have no conflict of interest.

in regions adjacent to the infarct for weeks following stroke. These findings suggest that one mechanism of neurodegeneration following stroke is the failure of glial scars to impermeably segregate areas of liquefactive necrosis from surviving brain tissue.

Keywords

Chronic stroke; Neurodegeneration; Liquefactive necrosis; Glial scar; Inflammation

1. Introduction

Activated astrocytes respond rapidly to ischemic stroke by upregulating genes for intermediate filaments such as glial fibrillary acidic protein (GFAP), calcium-binding protein B (S100B), vimentin, and nestin (Pekny and Nilsson, 2005; Farina et al., 2007; Cekanaviciute and Buckwalter, 2016). These changes in gene expression are accompanied by proliferation and migration towards the injured area. The injury is then walled off by a front line of reactive astrocytes interspersed with activated microglia/macrophages, resulting in a glial scar. The physical barrier function of the glial scar is reinforced by the production of extracellular matrix proteins such as fibronectin, laminin, and chondroitin sulphate proteoglycans (Cekanaviciute and Buckwalter, 2016). Together, these mechanisms create a barrier that corrals inflammatory cells present within the core of the injury (Bush et al., 1999; Wanner et al., 2013). However, it is currently unknown how effectively glial scars sequester the potentially neurotoxic extracellular fluid present within chronic CNS infarcts.

The extracellular fluid within chronic CNS infarcts is potentially neurotoxic because of the unique way in which infarcts within the CNS resolve. Unlike other tissues, the brain responds to ischemia by undergoing liquefactive necrosis. Liquefactive necrosis occurs in abscesses throughout the body, and is usually caused by an inflammatory response to infection. However, liquefactive necrosis occurs in the brain in response to stroke or other trauma, even in the absence of infection (Robbins et al., 2010).

Liquefactive necrosis is characterized by the degradation of tissue, and its transformation to a liquefactive mass. It persists for many months following stroke and other brain injuries, is largely uncharacterized in terms of its constituents and toxicity to surrounding brain regions, and the exact time frame of its resolution is unknown. The eventual outcome of liquefactive necrosis is cystic encephalomalacia, the term given to the end stage of infarct resolution when all that remains is an area of astrogliosis and a cerebrospinal fluid (CSF) filled cavity (Nguyen et al., 2016).

Until the stage of cystic encephalomalacia is reached, how effectively stroke infarcts are compartmentalized away from uninfarcted tissue has relevance for stroke recovery. This is because more than one-third of stroke survivors subsequently develop dementia (Barba et al., 2000; Leys et al., 2005; Bejot et al., 2011) and the cause or causes of this dementia are unclear. One potential mechanism that has not been investigated before is the possibility that glial scars only partially segregate neurotoxic extracellular fluid present within areas of liquefactive necrosis from the rest of the brain during recovery.

Although the stage of liquefactive necrosis is largely uncharacterized, it is known that in both mice and humans, infarcts at the stage of liquefactive necrosis are sites of chronic inflammation (Doyle et al., 2015; Nguyen et al., 2016). In C57BL/6 mice we recently demonstrated with our colleagues that this inflammation includes a chronic B-lymphocyte response in the infarct and an increased concentration of antibodies in the surrounding brain tissue for months after the injury (Doyle et al., 2015). We replicated this finding in multiple mouse models of stroke. Importantly, in one of these models, in which the infarct is located adjacent, but not incorporating the hippocampus, mice developed delayed cognitive deficits (Doyle et al., 2015).

As an indication to how effectively infarcts in the CNS are compartmentalized away from uninfarcted tissue, we did not detect B-lymphocytes and plasma cells in the brain outside of the stroke infarct in any of the stroke models we evaluated (Doyle et al., 2015). However, although the B-lymphocytes and plasma cells remained within the infarcts, it appeared that the antibodies produced by the plasma cells crossed the glial scar and infiltrated the surrounding brain tissue in the weeks after stroke. These results suggest that glial scars fail to completely contain potentially neurodegenerative molecules being produced, or otherwise present within CNS infarcts such as autoreactive antibodies (Ankeny et al., 2009; Ankeny and Popovich, 2010).

The failure of glial scars to successfully contain neurodegenerative factors present in areas of liquefactive necrosis has important implications for individuals recovering from a CNS injury. It suggests that glial scar permeability may be a significant cause of the delayed brain atrophy and dementia seen in some patients following stroke. Therefore, in this study, we evaluated the toxicity of the extracellular fluid present in areas of liquefactive necrosis following stroke, and determined how effectively, and by which mechanisms, neurodegenerative factors present in areas of liquefactive necrosis are sequestered from the surviving brain tissue.

2. Materials and methods

2.1. Mice

Adult 3–5-month-old C57BL/6 and BALB/c male mice were purchased from the Jackson Laboratory. Animals were housed under a 12-hour light/dark schedule with ad libitum access to food and water. All procedures met the National Institute of Health guidelines with approval from the University of Arizona Institutional Animal Care and Use Committee. For euthanasia, mice were intraperitoneally injected with a cocktail of 100 mg/kg ketamine, 20 mg/kg xylazine, and 3 mg/kg acepromazine, followed by intracardial perfusion with 0.9% saline. Brains were extracted, and either snap frozen in liquid nitrogen for biochemical assays, post-fixed in 4% paraformaldehyde (PFA) and cryoprotected in 30% sucrose for sectioning on a freezing microtome, or immersed in 2.5% glutaraldehyde and 2% PFA for electron microscopy.

2.2. Stroke surgeries

Distal middle cerebral artery occlusion (DMCAO) plus hypoxia (DH stroke) was performed on C57BL/6 mice, as previously described (Doyle et al., 2012; Nguyen et al., 2016). Mice were anesthetized by isoflurane inhalation, and an incision was made to expose the temporalis muscle. A pocket was created in the muscle to expose the skull underneath, and the right MCA identified. A microdrill was used to expose the underlying MCA. The meninges were cut, and the vessel cauterized using a small vessel cauterizer. The wound was then closed using surgical glue. Immediately following surgery, mice were placed in a large chamber containing 9% oxygen and 91% nitrogen for 45 min. Sham mice underwent the same surgical steps, except for cauterization of the MCA, and were also given 9% oxygen and 91% nitrogen for 45 min immediately after surgery. Core body temperature was maintained at 37 °C throughout surgery and hypoxia. Mice were randomly allocated into stroke and sham experimental groups. This stroke model creates a large infarct comprising approximately 25% of the stroked hemisphere, has little variability, and excellent long-term survivability (Doyle et al., 2012). Hypoxia is necessary with this model because C57BL/6 mice that undergo DMCAO without hypoxia have significantly smaller infarcts (Doyle et al., 2012). BALB/c mice underwent DMCAO without hypoxia, as previously described (Doyle et al., 2012; Nguyen et al., 2016). DMCAO by itself generates an infarct in BALB/c mice that is equivalent in size and location to the infarct generated by DH stroke in C57BL/6 mice (Doyle et al., 2012). To induce photothrombotic stroke, C57BL/6 mice were injected intraperitoneally with 100 mg/kg Rose Bengal (Millipore Sigma, Cat. No. 330000) dissolved in 0.9% saline. Thirty minutes following injection, mice were anesthetized by isoflurane inhalation, and an incision was made on the top of the head to expose the skull. An optic cable connected to a metal halide fiber optic illuminator (Dolan-Jenner MH-150; Edmund Optics) was then placed on top of the skull using a stereotactic frame, and the light source was turned on for 20 min.

2.3. Immunostaining

Coronal sections (40 μm) were taken through the entire brain using a freezing Microm HM 450 sliding microtome (Thermo Fisher Scientific). Free floating sections were then immunostained using standard techniques (Doyle et al., 2015; Nguyen et al., 2016). The following primary antibodies were used: immunoglobulin (IgG; Vector Laboratories, Cat. No. BA2000, RRID: AB2313571), glial fibrillary acidic protein (GFAP; Millipore Sigma, Cat. No. AB5541, RRID: AB177521), CD68 (Bio-Rad, Cat. No. MCA1957GA, RRID: AB324217), claudin-5 (Thermo Fisher Scientific, Cat. No. 352588, RRID: AB2532189), B220 (BD Biosciences, Cat. No. 553085, RRID: AB394615), CD3 (BD Biosciences, Cat. No. 550277, RRID: AB393573), lysosomal associated membrane protein-1 (LAMP-1; abcam, Cat. No. AB25245, RRID: AB449893), ionized calcium-binding adapter molecule 1 (Iba1; Wako, Cat. No. 019-19741, RRID: AB839504), matrix me-tallopeptidase (MMP)-9 (abcam, Cat. No. AB38898, RRID: AB776512), chondroitin sulphate proteoglycan (NG2; Millipore Sigma, Cat. No. AB5320, RRID: AB11213678), CD31 (abcam, Cat. No. 28364, RRID: AB726362), neuronal nuclei (NeuN) (Millipore Sigma, Cat. No. MAB377, RRID: AB2298772), and choline acetyltransferase (ChAT; Millipore Sigma, Cat. No. AB144P, RRID: AB2079751). Sections were then labeled with the appropriate secondary antibody in conjunction with ABC Vector Elite and 3,3′-diaminobenzidine kits (Vector Laboratories)

for visualization under a Motic BA410 light microscope coupled with a MoticamPro 282A camera or a Keyence BZ-X700 digital microscope with phase contrast, light, and fluorescence capabilities. For confocal or epifluorescence imaging, sections were incubated in Alexa Fluor secondary antibodies (Thermo Fisher Scientific), and captured with a Leica SP5-II laser scanning confocal microscope or a Leica DMI6000 epifluorescence microscope.

2.4. Nissl staining

Mounted, dehydrated tissue sections were cleared in xylenes, rehydrated, immersed in 0.5% cresyl violet acetate (Millipore Sigma, Cat. No. C5042) solution for 1 min, rinsed with distilled water, differentiated in 0.25% acetic alcohol, dehydrated through graded ethanol series, cleared, and coverslipped.

2.5. Quantification of neovascularization following stroke

Tissue sections were stained with hematoxylin and eosin (H&E; VWR, Cat. No. 95057-844 and 95057-848) according to standard techniques. Two sections per mouse (n = 4 mice per experimental group) were analyzed. Blood vessel density (per μm^2 of infarct) was then assessed by manually counting the number of blood vessels within each infarct per mouse, using a 20× objective, at bregma −1.94 and −0.02 mm, as well as the equivalent area in the somatosensory cortex on the contralateral hemisphere.

2.6. Determination of blood brain barrier permeability

To evaluate blood brain barrier (BBB) integrity following stroke, mice (n = 5 per experimental group) were intraperitoneally injected with 2% Evans Blue (Millipore Sigma, Cat. No. E2129) dissolved in 0.1 M phosphate buffer saline (PBS) at 24 h, 1 week, or 7 weeks following stroke or sham surgery. Mice were perfused 3 h later. Brains were photographed, and extravasation into each brain hemisphere was measured colorimetrically, as previously described (Radu and Chernoff, 2013).

2.7. Electron microscopy

2.7.1. Mouse brain tissue—Brains used for transmission and scanning electron microscopy (EM) were fixed in 2.5% glutaraldehyde and 2% PFA in 0.1 M Pipes buffer for 1 h at room temperature, or overnight at 4 °C. Following washes in 0.05 M Pipes buffer and 0.05 M glycine, and washes in 0.1 M Pipes buffer, dissected stroke regions from each brain were then post-fixed in 1% osmium tetroxide for 1 h. After fixation, samples underwent washes in deionized water (DIW). Samples for transmission EM were then block stained in 2% aqueous uranyl acetate, washed in DIW, dehydrated through a graded series of alcohols, infiltrated with 1:1 alcohol and Spurr's resin overnight, and then embedded in 100% Spurr's resin overnight at 60 °C. Samples for scanning EM were dehydrated, incubated in hexamethyldisilazan, and then air dried. Sections for transmission EM were viewed under an FEI Tecnai Spirit microscope operated at 100 kV. Eight-bit TIFF images were captured using an AMT 4 Mpixel camera. Sections for scanning EM were gold coated, and viewed under a FEI Company Inspect S microscope operated at 30 kV.

2.7.2. Human brain tissue—A chronic stroke infarct dissected from fresh frozen brain tissue (5-gram block) was obtained from the Banner Sun Health Research Institute (Sun City, AZ) (Beach et al., 2015). Chronic stroke was confirmed by both a clinical and neuropathological diagnosis. The sample was processed for EM, as described for mouse samples.

2.8. Multiplex immunoassays

Snap-frozen brain tissue samples were sonicated in ice-cold 0.1 M PBS containing 1% triton-X and 0.1% sodium deoxycholate, Protease Inhibitor Cocktail (1:100; Millipore Sigma), and Phosphatase Inhibitor Cocktail 2 (1:100; Millipore Sigma). Following centrifugation, the total protein concentration of each supernatant was measured using a Direct Detect Infrared Spectrometer (Millipore Sigma). Total immunoglobulin G (IgG), matrix metalloproteinases (MMPs), albumin, and cytokines and chemokines were then quantified using mouse multiplex magnetic bead kits purchased from Thermo Fisher Scientific and Millipore Sigma, and used according to the manufacturer's recommendations. Each lysate sample, standard, and quality control was measured in duplicate. Plates were read using a MAGPIX instrument (Luminex), and results were analyzed using MILLIPLEX Analyst 5.1 software (Millipore Sigma).

2.9. Extracellular fluid isolation

Under aseptic conditions and performed quickly on ice, extracellular fluid was harvested by dissecting (i) the 7-week-old infarct and (ii) the equivalent area of the contralateral cortex from C57BL/6 mice (n = 10) that had undergone DH stroke, and placing the dissected tissue into two sterile 15 ml conical centrifuge tubes containing 750 μl of the same cell culture media that was used for the subsequent primary neuron cultures (serum-free Neurobasal media, 1× B27 supplement, L-glutamine, and penicillin/streptomycin, without protease/phosphatase inhibitors; Thermo Fisher Scientific). For each region, the dissected tissue from each C57BL/6 mouse was pooled into one conical tube, which eventually contained 10 dissected infarcts from all 10 mice; the second conical tube contained the dissected equivalent area of the contralateral cortex from all 10 mice. The pooled tissue was gently triturated by passage through a sterile P1000 micropipette (cut with 3 size openings: 30 times passage through the largest size opening, 20 times passage through the medium size opening, and 20 times passage through the smallest size opening). Dissociated cells were centrifuged at 300 rpm for 10 min at 4 °C. 10 μl of the supernatant was pipetted onto a hemocytometer to confirm the absence of cells under phase contrast microscopy. The remaining supernatant was collected and transferred into a new conical tube. The pellet was re-suspended in 750 μl of fresh culture media, followed by gentle trituration with a P1000 pipet (10 times passage through the largest size opening), and re-centrifuged at 300 rpm for 10 min at 4 °C. 10 μl of this supernatant was pipetted onto a microscope slide and viewed under phase contrast to confirm once again the absence of cells. The remaining supernatant was collected and combined with the supernatant from the first trituration. The pellet was resuspended in fresh culture media, and 10 μl was treated with a LIVE/DEAD viability/cytotoxicity assay (Thermo Fisher Scientific, Cat. No. L3224), according to the manufacturer's directions, to quantify the percentage of cell lysis resulting from the trituration process. We found that mechanical dissociation caused an average of 7.7% cell

death (stained by ethidium homodimer-1 as a marker for cell death and calcein-AM as a marker for cell viability) in the pellets generated from the infarcts, and an average of 8.6% cell death in the pellets generated from the equivalent areas of the control contralateral cortices. The protein concentrations of the infarct supernatant and the contralateral cortex supernatant were then measured via a Direct Detect spectrometer, and normalized to 4 mg/ml of total protein. The extracellular fluid samples were then stored at −80°C until treatment. The isolation of extracellular fluid was repeated in three separate experiments (n = 3 sets of biological samples), with the exception that for the second and third repeat, the infarct and contralateral cortex were dissected from 5 mice and triturated in 350 μl of culture media.

2.10. Primary neuronal cultures and cell survival assays

Primary cortical and hippocampal neuron cultures were prepared from timed-pregnant C57BL/6 mice on embryonic day 16 (E16) and allowed to mature for 7 days, as previously described (Yang et al., 2006; Yang et al., 2008; Yang et al., 2016), before experimentation. Tissue culture wells were coated with 10 μg/mL poly-L-lysine in 0.1 M PBS. Cells were incubated in DMEM/F12 containing 10% fetal bovine serum for the first 2–4 h, and subsequently maintained in serum-free Neurobasal media with 1× B27 supplement, L-glutamine, and penicillin/streptomycin (Thermo Fisher Scientific). Neurons were seeded in 24-well plates at a density of 30,000–40,000 cells per well, and allowed to mature for 7 days. Cell survival following 4 hour exposure to extracellular fluid isolated from either the chronic stroke infarcts or the equivalent area of the contralateral cortex was measured by using the ViaLight Plus Bioassay kit (Lonza, Cat. No. LT07), according to the manufacturer's instructions. This highly sensitive assay allows for the bioluminescent detection of cellular ATP as a measure of viability (i.e., the number of living cells in culture). Cortical neurons received a 1:4 dilution of each of the 4 mg/ml extracellular fluid samples. Hippocampal neurons received either a 1:1, 1:4, or 1:9 dilution of each of the 4 mg/ml extracellular fluid samples. Control wells were treated with culture media as a negative control, and 500 μM (for the 1:1 dilution) of monosodium glutamate (MSG) as a positive control. Samples were run in quadruplicate and the cell survival assay experiment was repeated in 3 independent neuron preparations.

2.11. Dextran injections

To determine the permeability of the glial scar, 7-week-old and 12-week-old DH stroke infarcts (n = 3 mice per experimental group) were stereotactically injected with 1 μl FITC-labeled dextrans (0.1 mg/μl) at a rate of 0.1 μl/min, penetrating 0.2 mm into the area of liquefactive necrosis (molecular weights: 10,000 and 70,000 Da; Thermo Fisher Scientific). These dextrans have covalently bound lysine residues that permit them to be conjugated to surrounding biomolecules by 4% PFA mediated fixation for subsequent detection by fluorescence microscopy. The injection was performed surgically through the original craniotomy while mice were under general anesthesia. Mice were sacrificed at 6 h, 12 h, and 24 h post-injection. Mice (n = 7) that underwent photothrombotic stroke were also injected with the 10,000 dalton dextran at 7 weeks post-stroke through a new craniotomy exposing the infarct. These mice were sacrificed at 12 h post-injection. To determine the permeability of the blood vessels in the peri-infarct location, mice (n = 3–4 per group) were

also injected into the circulation via intraperitoneal injection with 250 μl Texas Red-labeled dextrans (8 mg/ml) (molecular weight: 10,000 Da; Thermo Fisher Scientific), and were sacrificed at 20 min, 6 h, 12 h, and 24 h post-injection following 7 weeks post-stroke. Post-hoc Nissl staining was used to confirm that the stereotaxic injection into the infarct through the original craniotomy did not damage or penetrate the glial scar. To quantify dextran endocytosis in the glial scar, dextran positive cells were counted, and the percentage that were double positive for either GFAP or Iba1 was determined. Counts from multiple fields of view within the glial scar for each animal were averaged to generate a single value per mouse.

2.12. Quantitative evaluations of brain atrophy, hippocampal enlargement, and neuron loss

Atrophy of the ipsilateral hemisphere was evaluated by calculating the volume of each hemisphere through manual tracing using ImageJ analysis software (NIH) in 6 brain sections (40 μm thick and 1 mm apart) per mouse (n = 3–7 mice per experimental group) that underwent DH stroke or sham surgery, or were untreated (naive). Stroked mice were euthanized at 3 days, 1 week, or 12 weeks following surgery, and sham mice were euthanized at 12 weeks following surgery. Data is presented as the ratio of the volume of the ipsilateral hemisphere/contralateral hemisphere. To quantify hippocampal enlargement, measurements of hippocampal regions CA1–3 in Nissl stained tissue were obtained (n = 3–7 mice per experimental group). To quantify neuron loss, ChAT+ neurons were counted with an automated (Analyze Particles) function using ImageJ analysis software in the cortex adjacent to the infarct, as well as in the equivalent contralateral cortical region. Two sections per mouse (n = 3–7 mice per experimental group), and one 10× field containing the motor/somatosensory areas of each hemisphere between bregma −0.46 mm and −1.94 mm per section were analyzed. Data is presented as the ratio of the number of ChAT+ neurons in the ipsilateral/contralateral hemisphere. As an additional measure of neuron loss, the ratio of the percentage of the area stained by NeuN+ cells in multiple peri-infarct locations (peri-infarct cortex, hippocampus, striatum, and external capsule) was measured using ImageJ analysis software and compared to the equivalent locations on the contralateral hemisphere. Both the peri-infarct cortex and striatum were measured at bregma 0.02, while the hippocampus and external capsule were measured at −1.94 (n = 4–6 mice per experimental group).

2.13. Statistical analysis

Multiplex immunoassays were performed with blinding to experimental condition. However, blinding was not possible for immunostaining experiments because of the infarct being visible in stroked mice. Data are expressed as mean ± standard error of the mean (SEM). Statistical analyses were performed with Prism 6.0 software (GraphPad), with the level of significance set at $p < .05$. Differences in blood vessel density were analyzed using a one-way ANOVA, in conjunction with Tukey's multiple comparisons post hoc method. Measurement of Evans Blue extravasation was assessed by a Student's *t*-test. For multiplex immunoassay experiments, differences in protein concentrations in experiments with two experimental groups were analyzed by a Student's *t*-test. Differences in protein concentrations in experiments with three or more experimental groups were analyzed by one-way ANOVA. For the extracellular fluid toxicity experiment, the data were analyzed using a one-way ANOVA per dilution, followed by Tukey's multiple

comparisons post hoc test. Measurements of dextran leakage and endocytosis in the glial scar were analyzed using a two-way ANOVA, followed by Sidak's multiple comparisons post hoc method. Atrophy of the ipsilateral hemisphere in the weeks following DH stroke was assessed by one-way ANOVA, followed by Sidak's multiple comparisons post hoc method. ChAT immunohistochemistry data were analyzed using a Student's *t*-test and NeuN immunohistochemistry data were analyzed using one-way ANOVA.

3. Results

3.1. Neovascularization following stroke results in a population of leaky microvessels

Prior to assessing the overall toxicity of the extracellular fluid present in areas of liquefactive necrosis, and the barrier properties of glial scars following a stroke model of CNS injury, we sought to further characterize the stage of liquefactive necrosis, with the goal of evaluating what potentially neurotoxic factors are present during this stage of chronic infarction.

A study by Yu and colleagues using an alternative stroke model reported that stroke results in the formation of a network of leaky blood vessels within the infarct (Yu et al., 2007). To confirm this finding using our DH stroke (DMCAO plus hypoxia) model, we performed both H&E histological staining (Fig. 1A) and anti-CD31 (platelet endothelial cell adhesion molecule-1, PECAM-1; Fig. 1B) immunostaining to assess neovascularization following stroke. An Evans Blue permeability assay was then performed to assess the extent to which the new blood vessels are leaky (Fig. 1D). Both H&E staining (Fig. 1A) and CD31 immunoreactivity (Fig. 1B) confirmed that a network of microvessels forms in the infarct in the first week after DH stroke. Quantitation revealed that although there was significant regression of these vessels between 1 week and 2 weeks, vessel density was still significantly increased at 7 weeks compared to 24 h following stroke (Fig. 1C, left graph). There was no significant change in blood vessel density in the contralateral hemisphere at any time point following stroke (Fig. 1C, right graph).

To determine whether the newly formed blood vessels mature into vessels with full BBB competency, mice were injected intraperitoneally with Evans Blue at 24 h, 1 week, and 7 weeks following stroke, and then perfused with 0.9% saline 3 h following injection. Evans Blue binds to albumin (67 kDa), and therefore its concentration in the brain is a measure of albumin extravasation (Radu and Chernoff, 2013). Evans Blue concentration in the infarcted hemisphere compared to the equivalent area of the contralateral hemisphere, as measured by visual inspection and colorimetric assay, revealed that although the integrity of the BBB was largely restored between 24 h (left graph and image) and 1 week (middle graph and image) after stroke, a small, but significant amount of Evans Blue/albumin still leaks into the ipsilateral hemisphere when injected 7 weeks (right graph and image) after stroke (Fig. 1D). These results suggest that chronic stroke infarcts may contain molecules and proteins present in the circulation that are associated with neurodegeneration when their entry into the CNS is dysregulated. Examples of circulating factors associated with neurodegeneration include albumin, homocysteine, complement proteins, cholesterol, autoantibodies, and transferrin (Zecca et al., 2004; Koudinov and Koudinova, 2005; Obeid and Herrmann, 2006; Ankeny et al., 2009; Hooper et al., 2009; Iadecola, 2010).

Next, we sought to determine the cause of why blood vessels within stroke infarcts are chronically leaky to molecules present in the plasma. Astrocytic end-feet typically provide complete coverage of the cerebral microvasculature in the normal, intact brain (Mathiisen et al., 2010), and are important for neurovascular unit function (Abbott et al., 2006). However, although chronic infarcts are encapsulated by astrocytes, GFAP+ staining showed that they contain very few astrocytes within (Fig. 2A). Therefore, blood vessels that form in the infarct in the aftermath of stroke appear to be largely devoid of astrocyte support. We also performed an NG2 immunostain to determine whether NG2+ pericytes are present on the blood vessels that form within the area of liquefactive necrosis following stroke. Although there was extensive NG2+ labeling throughout the brain of both pericytes and polydendrocytes, there was very little NG2+ staining within the core of the infarct (Fig. 2B).

Moreover, levels of matrix metalloproteinases (MMPs), which are known to disrupt tight junctions (Yang et al., 2007), were significantly elevated in chronic stroke infarcts (Fig. 2C). Specifically, we discovered high concentrations of MMP2, MMP3, and MMP8 in stroke infarcts at 7 weeks following stroke by multiplex immunoassays. Furthermore, we also observed high expression of MMP9 in stroke infarcts at 7 weeks following stroke by immunostaining (Fig. 2D). Immunostaining for claudin-5, a constituent of tight junctions in the CNS, provided additional support that there is a paucity of tight junctions in blood vessels within chronic stroke infarcts (Fig. 2E).

Together, these findings demonstrate that stroke infarcts contain leaky blood vessels for at least 7 weeks following stroke, and that the leakiness of these vessels correlates with a lack of astrocyte support, a scarcity of tight junctions, and elevated expression of MMPs, which are known to interfere with tight junction formation and function. In short, areas of liquefactive necrosis are areas of chronic BBB compromise.

3.2. Stroke infarcts are sites of chronic inflammation

We recently provided evidence that infarcts at the stage of liquefactive necrosis are sites of chronic inflammation (Doyle et al., 2015; Nguyen et al., 2016). Here, we validated these findings, while also including additional markers of neuroinflammation, by performing immunostaining and multiplex immunoassays on brain tissue harvested from mice 7 weeks following stroke. As shown in Fig. 3A, LAMP-1 and Iba1 immunofluorescence confirmed that even at 7 weeks following stroke, infarcts are sites of chronically activated microglia/macrophages. Additionally, the presence of substantial CD3 and B220 immunoreactivity in the infarcts corroborated that they are also sites of chronic T-lymphocyte (Fig. 3B) and B-lymphocyte (Fig. 3C) responses, respectively. Multiplex immunoassays confirmed that chronic infarcts are also sites of sustained pro-inflammatory cytokine and chemokine expression (Fig. 3D). Specifically, there was significant elevation of IL-1α, IL-1β, IL-3, IP-10, IL-5, TGFβ, IL-12 (p40), IL-12 (p70), IL-17, IL-13, RANTES, IFNγ, GM-CSF, TNFα, MIP-1α, MCP-3, EOTAXIN, and MCP-1 levels within the infarct of the stroked mice compared to the equivalent area of the cortex in sham mice. Of these, IL-1, IP-10, IL-17, IL-13, IFNγ, TNFα, EOTAXIN, and MCP-1 (CCL2) have all been linked to cytotoxicity in neurons (Gelbard et al., 1993; Sui et al., 2006; Takeuchi et al., 2006;

Thornton et al., 2006; Mizuno et al., 2008; Tzartos et al., 2008; Park et al., 2009; Shichita et al., 2009; Yang et al., 2011; Kang et al., 2012; Parajuli et al., 2015) (Table 1).

Our data thus far, coupled with previously published findings (Yu et al., 2007; Doyle et al., 2015; Nguyen et al., 2016), demonstrate that not only are chronic stroke infarcts sites of leaky neovascularization, which is associated with neurodegeneration (Iadecola, 2010), but also sites of sustained pro-inflammatory responses, including the expression of multiple cytokines and chemokines linked to neurodegeneration. Therefore, stroke infarcts at the stage of liquefactive necrosis are environments rich in numerous factors connected with neurotoxicity and neurodegeneration.

3.3. The extracellular fluid in areas of liquefactive necrosis is neurotoxic

To directly test the neurotoxicity of the extracellular milieu present in areas of liquefactive necrosis, we isolated the extracellular fluid from 7-week-old stroke infarcts, and compared its toxicity to the toxicity of the extracellular fluid isolated from the equivalent area of the contralateral cortex. The extracellular fluid was isolated from each brain region using a combination of gentle trituration and low speed centrifugation, and was verified to be cell free by visualization with a hemocytometer under phase contrast microscopy. To control for cell lysis caused by the isolation procedure, we quantified cell death using markers of cell membrane integrity and enzymatic activity in the remaining pellet with a standard LIVE/DEAD viability/cytotoxicity assay, and ascertained that our technique resulted in an average of 7.7% cell death in the infarct samples, and an average of 8.6% cell death in the control samples.

The toxicity of each extracellular fluid sample was then tested separately in both primary cortical and hippocampal neurons after they were allowed to mature for 7 days in culture. Bioluminescent measurement of cellular ATP, using a cell cytotoxicity bioassay, revealed that within 4 h of treatment, the extracellular fluid isolated from the area of liquefactive necrosis was significantly more toxic to cortical (Fig. 4A) and hippocampal neurons (Fig. 4B) compared to the same dilution (1:1, 1:4, and/or 1:9) of extracellular fluid isolated from the contralateral cortex.

3.4. Glial scars are permeable barriers

It is unlikely that tight junctions connect glial scar astrocytes. This is because despite decades of research into the localization of tight junctions within the CNS, glial scar astrocytes have yet to be reported to connect to each other via this mechanism. If glial scar astrocytes do not connect to each other with tight junctions, then glial scars are unlikely to form an impermeable physical barrier to neurodegenerative factors present within chronic stroke infarcts. Therefore, we next evaluated the ultrastructure of the glial scar to visualize how the astrocytes that comprise the physical front line of glial scars are inter-connected.

Scanning EM revealed glial scars in mice to be primarily comprised of twisted bundles of hypertrophied astrocytic processes, oriented parallel to the infarct, as previously described (Fig. 5A) (Wanner et al., 2013). Scanning EM in conjunction with CD3 immunostaining also revealed that glial scars contain T-lymphocytes (Fig. 5B). This supports a previous finding by Wanner and colleagues who demonstrated that glial scars corral CD45+ inflammatory

cells (Wanner et al., 2013). As expected, we found no evidence of tight junctions between astrocytes in the location of glial scars by transmission EM (Fig. 5C). Scanning EM of human stroke tissue demonstrated that the structure of the glial scar in humans is similar to the structure of the glial scar in mice. The human glial scar is also comprised of twisted bundles of hypertrophied processes oriented parallel to the infarct (Fig. 5D).

Having confirmed by transmission EM that glial scars are not tight junction barriers, we proceeded to assess the extent to which they are permeable to molecules present within areas of liquefactive necrosis. Previously, we demonstrated that within 7 weeks of stroke, isotype switched plasma cells are present within the infarct, and antibodies accumulate in the hippocampus adjacent to the infarct (Doyle et al., 2015). We provided evidence that the antibodies that leak into the uninfarcted tissue are from plasma cells in the infarct by showing that the ratio of the different antibody isotypes in the parenchyma matches the ratio of the isotypes in the area of liquefactive necrosis, but is different from the ratio of the isotypes in the plasma (Doyle et al., 2015). We also showed that the ratio of the isotypes in the parenchyma changes between 1 week and 7 weeks following stroke, suggesting that antibody leakage into uninfarcted brain regions from areas of liquefactive necrosis is a continuous process (Doyle et al., 2015).

To corroborate these findings, we performed immunostaining for IgG on tissue harvested at 1 week and 7 weeks following DH stroke. As previously shown in Fig. 3C, B-lymphocytes were restricted to the location of the infarct and were not present in the adjacent brain tissue. However, IgG immunoreactivity appeared as a diffuse cloud around the area of liquefactive necrosis at both time points (Fig. 6A). The radiation of IgG from the area of liquefactive necrosis was also apparent in another strain, BALB/c mice, following DMCAO without hypoxia (Fig. 6B). These findings suggest that antibodies leak into the brain from areas of liquefactive necrosis.

To quantify the extent of putative antibody leakage across the glial scar, we performed a multiplex immunoassay on tissue harvested from C57BL/6 mice at 7 weeks following DH stroke. Results revealed that the concentration of total IgG was approximately 3-fold higher in the area adjacent to the infarct at 7 weeks following stroke compared to the contralateral hemisphere (Fig. 6C). The data also revealed that the concentration of IgG in the infarct was 4.5-fold higher than the concentration in the area adjacent to the infarct (Fig. 6C). These findings suggest that while glial scars are permeable to antibodies, they are still robust physical barriers to their diffusion.

Additionally, we performed an immunoassay to quantify the extent of putative albumin leakage across the glial scar on tissue harvested at 7 weeks following DH stroke. Quantitation showed that the concentration of albumin was significantly increased in the area adjacent to the infarct at 7 weeks following stroke compared to the equivalent location in the contralateral hemisphere (Fig. 6D).

To determine if leakage from blood vessels in the peri-infarct location could be the source of the increased IgG and albumin present in the area adjacent to the infarct, we injected a 10 kDa Texas Red-labeled dextran into the circulation of C57BL/6 mice at 7 weeks post-DH

stroke and evaluated the extent of leakage from peri-infarct blood vessels at 20 min, 6 h, 12 h, and 24 h following injection. Although we observed that a diffuse cloud of the Texas Red-labeled dextran localized to peri-infarct vessels at the 6 hour, 12 hour, and 24 hour time points (Fig. 6E), we were unable to ascertain whether this diffusion effect was due to direct leakage from peri-infarct blood vessels, or alternatively was due to leakage from blood vessels within the infarct, followed by secondary leakage across the glial scar.

Therefore, to directly test how effectively glial scars segregate areas of liquefactive necrosis from adjacent brain tissue, mice were injected with a 10 kDa dextran into the area of liquefactive necrosis at 7 weeks following stroke, and were then euthanized 6, 12, and 24 h later. Nissl staining was performed on serial sections to confirm that the injections, which were performed through the original craniotomy, did not puncture the glial scar. Mice were excluded if there was visual evidence that the injection needle had penetrated into the parenchyma.

At each time point, the 10 kDa dextran was evident on the parenchymal side of the glial scar (Fig. 7A), suggesting that glial scars are permeable barriers. However, the 10 kDa dextran was concentrated at the location of the scar at the 6-hour and 12-hour time points (Fig. 7B). This observation provides further evidence that glial scars nevertheless perform a robust physical barrier function. The 10 kDa dextran was also concentrated at the location of the external capsule at the 12-hour time point suggesting that drainage through this less dense region of white matter fiber tracts occurs (Fig. 7A). Quantitation of the dextran indicated significant clearance of dextran from the parenchyma by 24 h post-injection (Fig. 7C).

To confirm that glial scar permeability is not stroke model specific, C57BL/6 mice also underwent photothrombotic stroke followed by 7 weeks of recovery. The 10 kDa dextran was injected into the infarct and mice were sacrificed 12 h later. Once more, the dextran was apparent on the parenchymal side of the glial scar (Fig. 7D).

To validate that larger molecules such as albumin (67 kDa) are capable of crossing glial scars, a separate group of mice were injected with a 70 kDa dextran into the area of liquefactive necrosis. For this experiment, mice were injected at 12 weeks following stroke, and then euthanized 24 h later. The 70 kDa dextran was detectable on the parenchymal side of the glial scar, with increased penetration in areas where the glial scar was comprised of fewer astrocytes (Fig. 7E).

3.5. Glial scars are endocytic barriers

Our transmission EM data suggested that glial scars may be endocytic barriers (Fig. 5C). To explore this observation in depth, we performed immunostaining with an antibody for scavenger receptor class D member 1 (CD68) to survey for endocytic vesicles within the glial scar (Fig. 8A). CD68 is also a member of the lysosomal/endosomal-associated membrane glycoprotein family (LAMP). CD68 immunostaining confirmed the presence of abundant lysosomes/endosomes within glial scars (Fig. 8A). Confocal microscopy of the glial scar from each mouse injected with the 10 kDa or 70 kDa dextrans also indicated that glial scars are endocytic barriers (Fig. 8B). Quantification of the colocalization of the 10 kDa dextran with GFAP+ and Iba1+ cells within the glial scar, visualized by confocal

microscopy, revealed that both of these cell types had endocytosed the dextran, albeit the microglia/macrophages had endocytosed the dextran to a significantly greater extent than the astrocytes at every time point (Fig. 8C). Furthermore, LAMP-1 immunostaining (Fig. 8D) and quantitation (Fig. 8E) confirmed a significant increase in LAMP-1 expression within both glial scar astrocytes and glial scar microglia/macrophages.

3.6. Material leaking across the glial scar is cleared by both the paravascular clearance and microglial endocytosis

To elucidate the mechanism(s) of clearance of material leaking across the glial scar, we next tracked the localization of the 10 kDa dextran within the parenchyma at 6, 12, and 24 h following injection (Fig. 9A). At each time point, the dextran localized to the paravascular space in between the lumen of blood vessels and the astrocytes that envelope them. This particular localization of the dextran indicates that parenchymal diffusion coupled to convective or dispersive flow in the paravascular spaces is a mechanism of clearance (Fig. 9B) (Iliff et al., 2013; Smith et al., 2017). A representative scanning EM image of an astrocyte/blood vessel interface in the ipsilateral hemisphere at 7 weeks following stroke is provided in Fig. 9C. At each time point, the dextran also localized to within parenchymal microglia, indicating microglial endocytosis is a second mechanism of clearance (Fig. 9D).

3.7. Delayed neurodegeneration occurs in brain regions surrounding areas of liquefactive necrosis

The preceding evidence indicates that factors associated with neurodegeneration leak into the brain through permeable glial scars for months following stroke. Although there are mechanisms of clearance, neurons in the parenchyma still come into contact with these factors. Therefore, we investigated whether leakage across the glial scar correlates with ongoing neurodegeneration in the weeks following DH stroke.

Brain sections from mice sacrificed at 72 h, 1 week, or 12 weeks post-stroke were stained with Nissl, and the ratio of the volume of the ipsilateral/contralateral hemisphere was calculated. The data revealed that there is significant atrophy of the ipsilateral hemisphere between 1 week and 12 weeks following stroke (Fig. 10A & B). This finding is particularly evident in the area of the ipsilateral cortex (motor/somatosensory cortex, layers I–VI) adjacent to the infarct, where substantial thinning occurs between these time points.

Nissl staining also revealed significant swelling of neuronal cell bodies in the ipsilateral hippocampus compared to the contralateral hippocampus of stroked mice, or the hippocampus of naive mice at 12 weeks post-stroke (Fig. 10C & D). This finding is indicative of cytotoxic edema. The hippocampus is not infarcted by DH stroke (Doyle et al., 2012; Doyle et al., 2015), therefore chronic edema in the hippocampus following DH stroke may be a premorbid cellular response resulting from failure of the glial scar to sequester neurotoxic factors present within the infarct (Liang et al., 2007).

To further assess for delayed neurodegeneration in the weeks following stroke, a ChAT immunostain for cholinergic neurons was performed on tissue from mice sacrificed at 1 week and 7 weeks following stroke. Cholinergic neurons and their projections to cortical and hippocampal targets are critical for attention and cognition, and are particularly vulnerable

in aging, neurodegenerative disease, and dementia (Davies and Maloney, 1976; Whitehouse et al., 1982). We found significant loss of ChAT+ neurons in the cortex adjacent to the infarct between 1 week and 7 weeks (Fig. 10E & F), indicating a delayed loss of cholinergic neurons in the motor/somatosensory cortex adjacent to the infarct. Neurodegeneration in the weeks following DH stroke was further confirmed by NeuN immunostaining. We saw a reduction of NeuN + staining in the peri-infarct cortex and external capsule, but not the striatum or hippocampus, between 1 week and 8 weeks following stroke (Fig. 10G & H), which was confirmed by quantitation (Fig. 10I).

Together, these data demonstrate that leakage of factors associated with neurodegeneration into the brain through permeable glial scars correlates with degeneration of neurons in adjacent brain regions in the weeks following stroke.

4. Discussion

Glial scars encircle damaged tissue after stroke and other injuries in the CNS, and are essential for repair (Wanner et al., 2013). They can take longer than two weeks to fully encapsulate infarcted tissue, and although they were long viewed as a barrier to regeneration, recent evidence indicate that they actually help rather than inhibit axonal regeneration (Anderson et al., 2016). The primary cellular constituents of glial scars are astrocytes and microglia/macrophages, with the border zone that interfaces with the infarct comprised of a frontline of elongated, hypertrophied astrocytes (Wanner et al., 2013).

The tissue enclosed by glial scars undergoes liquefactive necrosis (Robbins et al., 2010). Much less is known about the liquefactive necrosis stage of infarction than the acute stage of infarction, and infarcts are more typically referred to as chronic infarcts at this stage. However, there is a spectrum of pathology at the chronic stage of infarction and the term liquefactive necrosis allows differentiation between the stage when microglia/macrophages and proteolytic enzymes predominate, and the stage of cystic encephalomalacia, when all that is left is a CSF filled cavity surrounded by a glial scar border.

How long it takes for stroke infarcts to transition from the stage of liquefactive necrosis to the stage of cystic encephalomalacia is unknown, and the fact that up to one-third of stroke sufferers develop dementia raises the possibility that insufficient containment of the milieu in areas of liquefactive necrosis may be a cause of neurodegeneration in areas surrounding stroke infarcts (Kalaria et al., 2016). Although previous studies demonstrate that glial scars are effective at corralling CD45+ inflammatory cells (Wanner et al., 2013), how effectively they contain the extracellular fluid was undetermined.

Therefore, the first objective of this study was to further characterize the extracellular fluid present within chronic stroke infarcts during the stage of liquefactive necrosis, and to determine whether it is neurotoxic. The second objective was to determine how effectively glial scars seal the area of liquefactive necrosis following stroke, and to identify the cellular and molecular mechanisms involved. To accomplish these objectives, we used a mouse model of stroke in conjunction with an extracellular fluid toxicity assay, fluorescence and

electron microscopy, immunohistochemistry, tracer injections into the infarct, and multiplex immunoassays.

There was a strong rationale for the hypothesis that the extracellular milieu within areas of liquefactive necrosis is neurotoxic. Tissue around chronic stroke infarcts atrophies in the weeks and months following stroke (Skriver and Olsen, 1986; Skriver et al., 1990), there is BBB dysfunction in the infarct for months following stroke (Wardlaw et al., 2009; Topakian et al., 2010; Yang and Rosenberg, 2011), and in the mouse model of stroke that we used, in which the infarct is located adjacent to the hippocampus, the hippocampus develops a delayed deficit in long-term potentiation in the weeks following stroke (Doyle et al., 2015).

To isolate the extracellular fluid from the area of liquefactive necrosis, we developed a novel procedure designed to minimize cellular lysis and the release of DAMPs and endogenous proteases. Nevertheless, our isolation procedure resulted in approximately 8% cell death during the isolation in both the cells separated from the extracellular fluid in the area of liquefactive necrosis, and the cells separated from the extracellular fluid in the control cortex. While this demonstrates that the isolation procedure was similarly damaging to both types of tissue, each region consists of different cell populations. Therefore, the actual amount of DAMPs and proteases released by the extraction of the extracellular fluid from each region is likely to be discordant. With this limitation as a caveat, the extracellular fluid isolated from the area of liquefactive necrosis was substantially more toxic to neurons than the control extracellular fluid isolated from an equivalent area of the contralateral hemisphere using the same procedure.

The validity of our finding that the extracellular fluid present in the area of liquefactive necrosis is neurotoxic is bolstered by two probable explanations. First, we found that neovasculogenesis in the infarct results in a leaky population of microvessels in this location. This finding replicates results from other stroke models, where it has been proposed that neovascularization following stroke facilitates the transportation of peripheral immune cells to the area of damage to participate in the breakdown and removal of dead tissue (Manoonkitiwongsa et al., 2001; Yu et al., 2007). Although it has been proposed that this population of vessels is transient, the data we present here, as well as published data (Yu et al., 2007), demonstrate that their resorption following CNS injury is very gradual.

The presence of leaky blood vessels in the area of liquefactive necrosis signifies that the extracellular fluid in this location contains plasma. The dysregulated entry of plasma solutes into the brain is neurotoxic. For example, leakage of albumin into the brain is associated with epileptogenesis (Ivens et al., 2007; Weissberg et al., 2015). This finding is relevant to glial scar function because for a chronic undefined time period following CNS injury, blood vessels in areas of liquefactive necrosis leak plasma proteins, which then have a route into the brain through permeable glial scars. In support of the likelihood that this phenomenon happens in the weeks following stroke, we demonstrated here that (i) albumin leaks into areas of liquefactive necrosis for at least 7 weeks following stroke, (ii) a 70 kDa tracer with a similar molecular weight to albumin can leak across the glial scar, and (iii) the concentration of albumin in brain tissue adjacent to an area of liquefactive necrosis is higher than the concentration of albumin in an equivalent area in the contralateral hemisphere.

The presence of leaky blood vessels within chronic infarcts and permeable glial scars surrounding chronic infarcts has important implications for drug delivery following stroke. It suggests that drugs or compounds that target the prolonged inflammatory response within the infarct, as well as the vulnerable neurons that surround the infarct, can be delivered by systemic injection for months following stroke. Furthermore, because our data indicate that blood vessels in areas of liquefactive necrosis may be leaky due to high levels of MMP expression, these MMPs could be exploited for MMP activated drug targeting (Vartak and Gemeinhart, 2007). Additional experiments are required to determine the pharmacokinetics of drug penetration into areas of liquefactive necrosis, drug diffusion across glial scars, and to determine if the presence of MMPs can be exploited to help drug delivery to this location.

The second probable explanation for why the extracellular fluid in areas of liquefactive necrosis is more toxic to neurons than extracellular fluid isolated from control brain tissue, is that we show that this fluid contains MMPs, antibodies, and multiple cytokines and chemokines associated with neurotoxicity. A summary of their putative mode of toxicity is provided in Table 1. Most of these proteins, with the exception of antibodies, are between 10 and 70 kDa in size, which are the sizes of the fluorescent (dextran) tracers used in our experiments to evaluate glial scar permeability. It remains to be determined how the composition and toxicity of the extracellular fluid in the area of liquefactive necrosis changes over time, and how it is impacted by genetics and different stroke comorbidities.

With regard to glial scar permeability, we have shown that despite glial scars being both robust physical and endocytic barriers, they do not form a perfect seal. They are permeable to a 10 and 70 kDa tracer injected into the area of liquefactive necrosis for at least 12 weeks following stroke. With regard to the fate of molecules, such as these tracers, which leak across the glial scar, our data show that they are both endocytosed by microglia/macrophages in the adjacent tissue, as well as removed by a paravascular clearance mechanism. Importantly, even with these removal mechanisms, neurons in areas adjacent to sites of liquefactive necrosis are under a continuous mild assault for months following stroke. We propose that this is one cause of delayed neurodegeneration and brain atrophy following stroke.

It is of course unlikely that this is the only cause of delayed neurodegeneration following stroke. Physical disruption caused by the stroke disconnects many neurons and may cause transneuronal degeneration (Fornito et al., 2015). Physical disruption may also reduce the effectiveness of the paravascular space to remove metabolic waste products and other potentially neurotoxic interstitial solutes from the interstitial fluid in the ipsilateral hemisphere (Wang et al., 2017). These mechanisms almost certainly also contribute to delayed neurodegeneration following stroke.

The containment of the area of liquefactive necrosis is potentially improvable by therapeutic intervention. Following spinal cord injury, signaling by IL-6 and phosphorylated (p) STAT3 in reactive astrocytes is required for proper establishment of the glial scar (Okada et al., 2004; Wanner et al., 2013). Conversely, SOCS3 signaling interferes with the establishment of the glial scar (Okada et al., 2006; Hackett et al., 2016). It is likely that the pSTAT3/SOCS3 pathway also modulates formation of the glial scar in the brain following stroke.

Indeed, in support of this possibility, multiple research groups have reported a coordinated and long-lasting upregulation of gp130 mRNA and STAT3 activation in reactive astrocytes following cerebral ischemia (Suzuki et al., 2001; Choi et al., 2003; Raible et al., 2014). Therefore, targeting pSTAT3/SOCS3 signaling in the brain following stroke could be a method of accelerating and enhancing formation of the glial scar, and consequently creating a more robust barrier to sequester areas of liquefactive necrosis from uninfarcted tissue. Evidence that enhancing this containment may improve recovery comes from converse studies using mice in which proliferating astrocytes have been conditionally ablated. These mice have impaired recovery following CNS injury (Myer et al., 2006).

This study has several potential limitations. For example, we have not determined if the containment function of the glial scar is impacted by age. Whether age has an impact is significant because the average age of stroke sufferers is 68 years (Kissela et al., 2012). Future studies are needed to address whether older animals build a more robust glial scar, or if alternatively, glial scar formation is less coordinated and allows increased leakage of neurotoxic factors from the infarct into the surviving brain tissue. There is evidence for both possibilities. Although expression of the reactive astrocyte marker GFAP increases with aging (Nichols et al., 1993; Lee et al., 2000), as does reactive astrogliosis after injury (Badan et al., 2003), recovery from stroke is poorer in older animals (Badan et al., 2003).

Another possible limitation is that we have yet to interrogate the barrier function of each of the different extracellular matrix molecules present within glial scars. For example, astrocytes can produce four different types of proteoglycan: heparan sulphate proteoglycan, dermatan sulphate proteoglycan, keratan sulphate proteoglycan, and chondroitin sulphate proteoglycan (Silver and Miller, 2004), each of which may play a different role in sequestering the area of liquefactive necrosis from the rest of the brain during recovery from stroke. More research is needed to delineate the role of each component of the extracellular matrix in the containment function of glial scars.

In summary, these findings demonstrate that glial scars are not perfect repairs, and the incomplete sealing of sites of liquefactive necrosis allows entry of neurotoxic factors present in stroke infarcts into the surrounding parenchyma for months following stroke. To our knowledge this significant defect has not been previously explicitly recognized or investigated, and we propose that it has substantial implications for the delayed neurodegeneration and brain dysfunction seen months to years after stroke, as well as after other types of CNS injury.

Acknowledgments

This work was funded by NIH K99NR013593 (KPD), NIH R01NS096091 (KPD), NIH F31NS105455 (JCZ), the Phoenix Chapter of ARCS Foundation, Inc. (JCZ), and start-up funding provided by the University of Arizona, Tucson. We are grateful to the Banner Sun Health Research Institute for providing the human tissue sample. The Brain and Body Donation Program is supported by the National Institute of Neurological Disorders and Stroke (U24 NS072026 National Brain and Tissue Resource for Parkinson's Disease and Related Disorders), the National Institute on Aging (P30 AG19610 Arizona Alzheimer's Disease Core Center), the Arizona Department of Health Services (contract 211002, Arizona Alzheimer's Research Center), the Arizona Biomedical Research Commission (contracts 4001, 0011, 05-90, and 1001 to the Arizona Parkinson's Disease Consortium), and the Michael J. Fox Foundation for Parkinson's Research.

References

Abbott NJ, Ronnback L, Hansson E. 2006; Astrocyte-endothelial interactions at the blood-brain barrier. Nat Rev Neurosci. 7 :41–53. [PubMed: 16371949]

Anderson MA, Burda JE, Ren Y, Ao Y, O'Shea TM, Kawaguchi R, Coppola G, Khakh BS, Deming TJ, Sofroniew MV. 2016; Astrocyte scar formation aids central nervous system axon regeneration. Nature. 532 :195–200. [PubMed: 27027288]

Ankeny DP, Popovich PG. 2010; B cells and autoantibodies: complex roles in CNS injury. Trends Immunol. 31 :332–338. [PubMed: 20691635]

Ankeny DP, Guan Z, Popovich PG. 2009; B cells produce pathogenic antibodies and impair recovery after spinal cord injury in mice. J Clin Invest. 119 :2990–2999. [PubMed: 19770513]

Badan I, Buchhold B, Hamm A, Gratz M, Walker LC, Platt D, Kessler C, Popa-Wagner A. 2003; Accelerated glial reactivity to stroke in aged rats correlates with reduced functional recovery. J Cereb Blood Flow Metab. 23 :845–854. [PubMed: 12843788]

Barba R, Martinez-Espinosa S, Rodriguez-Garcia E, Pondal M, Vivancos J, Del Ser T. 2000; Poststroke dementia: clinical features and risk factors. Stroke. 31 :1494–1501. [PubMed: 10884443]

Beach TG, et al. 2015; Arizona study of aging and neurodegenerative disorders and Brain and Body Donation Program. Neuropathology. 35 :354–389. [PubMed: 25619230]

Bejot Y, Aboa-Eboule C, Durier J, Rouaud O, Jacquin A, Ponavoy E, Richard D, Moreau T, Giroud M. 2011; Prevalence of early dementia after first-ever stroke: a 24-year population-based study. Stroke. 42 :607–612. [PubMed: 21233464]

Bush TG, Puvanachandra N, Horner CH, Polito A, Ostenfeld T, Svendsen CN, Mucke L, Johnson MH, Sofroniew MV. 1999; Leukocyte infiltration, neuronal degeneration, and neurite outgrowth after ablation of scar-forming, reactive astrocytes in adult transgenic mice. Neuron. 23 :297–308. [PubMed: 10399936]

Cekanaviciute E, Buckwalter MS. 2016; Astrocytes: integrative regulators of neuroinflammation in stroke and other neurological diseases. Neurotherapeutics. 13 :685–701. [PubMed: 27677607]

Choi JS, Kim SY, Cha JH, Choi YS, Sung KW, Oh ST, Kim ON, Chung JW, Chun MH, Lee SB, Lee MY. 2003; Upregulation of gp130 and STAT3 activation in the rat hippocampus following transient forebrain ischemia. Glia. 41 :237–246. [PubMed: 12528179]

Davies P, Maloney AJ. 1976; Selective loss of central cholinergic neurons in Alzheimer's disease. Lancet. 2 :1403.

Doyle KP, Buckwalter MS. 2016; Does B lymphocyte-mediated autoimmunity contribute to post-stroke dementia? Brain Behav Immun. 64 :1–8. [PubMed: 27531189]

Doyle KP, Fathali N, Siddiqui MR, Buckwalter MS. 2012; Distal hypoxic stroke: a new mouse model of stroke with high throughput, low variability and a quantifiable functional deficit. J Neurosci Methods. 207 :31–40. [PubMed: 22465679]

Doyle KP, Quach LN, Sole M, Axtell RC, Nguyen TV, Soler-Llavina GJ, Jurado S, Han J, Steinman L, Longo FM, Schneider JA, Malenka RC, Buckwalter MS. 2015; B-lymphocyte-mediated delayed cognitive impairment following stroke. J Neurosci. 35 :2133–2145. [PubMed: 25653369]

Farina C, Aloisi F, Meinl E. 2007; Astrocytes are active players in cerebral innate immunity. Trends Immunol. 28 :138–145. [PubMed: 17276138]

Fornito A, Zalesky A, Breakspear M. 2015; The connectomics of brain disorders. Nat Rev Neurosci. 16 :159–172. [PubMed: 25697159]

Fujimoto M, Takagi Y, Aoki T, Hayase M, Marumo T, Gomi M, Nishimura M, Kataoka H, Hashimoto N, Nozaki K. 2008; Tissue inhibitor of metalloproteinases protect blood-brain barrier disruption in focal cerebral ischemia. J Cereb Blood Flow Metab. 28 :1674–1685. [PubMed: 18560439]

Gelbard HA, Dzenko KA, DiLoreto D, del Cerro C, del Cerro M, Epstein LG. 1993; Neurotoxic effects of tumor necrosis factor alpha in primary human neuronal cultures are mediated by activation of the glutamate AMPA receptor subtype: implications for AIDS neuropathogenesis. Dev Neurosci. 15 :417–422. [PubMed: 7835247]

Hackett AR, Lee DH, Dawood A, Rodriguez M, Funk L, Tsoulfas P, Lee JK. 2016; STAT3 and SOCS3 regulate NG2 cell proliferation and differentiation after contusive spinal cord injury. Neurobiol Dis. 89 :10–22. [PubMed: 26804026]

Hooper C, Pinteaux-Jones F, Fry VA, Sevastou IG, Baker D, Heales SJ, Pocock JM. 2009; Differential effects of albumin on microglia and macrophages; implications for neurodegeneration following blood-brain barrier damage. J Neurochem. 109 :694–705. [PubMed: 19187440]

Iadecola C. 2010; The overlap between neurodegenerative and vascular factors in the pathogenesis of dementia. Acta Neuropathol. 120 :287–296. [PubMed: 20623294]

Iliff JJ, Wang M, Zeppenfeld DM, Venkataraman A, Plog BA, Liao Y, Deane R, Nedergaard M. 2013; Cerebral arterial pulsation drives paravascular CSF-interstitial fluid exchange in the murine brain. J Neurosci. 33 :18190–18199. [PubMed: 24227727]

Ivens S, Kaufer D, Flores LP, Bechmann I, Zumsteg D, Tomkins O, Seiffert E, Heinemann U, Friedman A. 2007; TGF-beta receptor-mediated albumin uptake into astrocytes is involved in neocortical epileptogenesis. Brain. 130 :535–547. [PubMed: 17121744]

Kalaria RN, Akinyemi R, Ihara M. 2016; Stroke injury, cognitive impairment and vascular dementia. Biochim Biophys Acta. 1862 :915–925. [PubMed: 26806700]

Kang Z, Liu L, Spangler R, Spear C, Wang C, Gulen MF, Veenstra M, Ouyang W, Ransohoff RM, Li X. 2012; IL-17-induced Act1-mediated signaling is critical for cuprizone-induced demyelination. J Neurosci. 32 :8284–8292. [PubMed: 22699909]

Kang Z, Wang C, Zepp J, Wu L, Sun K, Zhao J, Chandrasekharan U, DiCorleto PE, Trapp BD, Ransohoff RM, Li X. 2013; Act1 mediates IL-17-induced EAE pathogenesis selectively in NG2+ glial cells. Nat Neurosci. 16 :1401–1408. [PubMed: 23995070]

Kissela BM, Khoury JC, Alwell K, Moomaw CJ, Woo D, Adeoye O, Flaherty ML, Khatri P, Ferioli S, De Los Rios La Rosa F, Broderick JP, Kleindorfer DO. 2012; Age at stroke: temporal trends in stroke incidence in a large, biracial population. Neurology. 79 :1781–1787. [PubMed: 23054237]

Koudinov AR, Koudinova NV. 2005; Cholesterol homeostasis failure as a unifying cause of synaptic degeneration. J Neurol Sci. 229–230 :233–240.

Lee CK, Weindruch R, Prolla TA. 2000; Gene-expression profile of the ageing brain in mice. Nat Genet. 25 :294–297. [PubMed: 10888876]

Leys D, Henon H, Mackowiak-Cordoliani MA, Pasquier F. 2005; Poststroke dementia. Lancet Neurol. 4 :752–759. [PubMed: 16239182]

Liang D, Bhatta S, Gerzanich V, Simard JM. 2007; Cytotoxic edema: mechanisms of pathological cell swelling. Neurosurg Focus. 22 :E2.

Manoonkitiwongsa PS, Jackson-Friedman C, McMillan PJ, Schultz RL, Lyden PD. 2001; Angiogenesis after stroke is correlated with increased numbers of macrophages: the clean-up hypothesis. J Cereb Blood Flow Metab. 21 :1223–1231. [PubMed: 11598500]

Mathiisen TM, Lehre KP, Danbolt NC, Ottersen OP. 2010; The perivascular astroglial sheath provides a complete covering of the brain microvessels: an electron microscopic 3D reconstruction. Glia. 58 :1094–1103. [PubMed: 20468051]

Mizuno T, Zhang G, Takeuchi H, Kawanokuchi J, Wang J, Sonobe Y, Jin S, Takada N, Komatsu Y, Suzumura A. 2008; Interferon-gamma directly induces neurotoxicity through a neuron specific, calcium-permeable complex of IFN-gamma receptor and AMPA GluR1 receptor. FASEB J. 22 :1797–1806. [PubMed: 18198214]

Mroczko B, Groblewska M, Barcikowska M. 2013; The role of matrix metalloproteinases and tissue inhibitors of metalloproteinases in the pathophysiology of neurodegeneration: a literature study. J Alzheimers Dis. 37 :273–283. [PubMed: 23792694]

Myer DJ, Gurkoff GG, Lee SM, Hovda DA, Sofroniew MV. 2006; Essential protective roles of reactive astrocytes in traumatic brain injury. Brain. 129 :2761–2772. [PubMed: 16825202]

Nguyen TV, Frye JB, Zbesko JC, Stepanovic K, Hayes M, Urzua A, Serrano G, Beach TG, Doyle KP. 2016; Multiplex immunoassay characterization and species comparison of inflammation in acute and non-acute ischemic infarcts in human and mouse brain tissue. Acta Neuropathol Commun. 4 :100. [PubMed: 27600707]

Nichols NR, Day JR, Laping NJ, Johnson SA, Finch CE. 1993; GFAP mRNA increases with age in rat and human brain. Neurobiol Aging. 14 :421–429. [PubMed: 8247224]

Obeid R, Herrmann W. 2006; Mechanisms of homocysteine neurotoxicity in neurodegenerative diseases with special reference to dementia. FEBS Lett. 580 :2994–3005. [PubMed: 16697371]

Okada S, Nakamura M, Mikami Y, Shimazaki T, Mihara M, Ohsugi Y, Iwamoto Y, Yoshizaki K, Kishimoto T, Toyama Y, Okano H. 2004; Blockade of interleukin-6 receptor suppresses reactive astrogliosis and ameliorates functional recovery in experimental spinal cord injury. J Neurosci Res. 76 :265–276. [PubMed: 15048924]

Okada S, Nakamura M, Katoh H, Miyao T, Shimazaki T, Ishii K, Yamane J, Yoshimura A, Iwamoto Y, Toyama Y, Okano H. 2006; Conditional ablation of Stat3 or Socs3 discloses a dual role for reactive astrocytes after spinal cord injury. Nat Med. 12 :829–834. [PubMed: 16783372]

Parajuli B, Horiuchi H, Mizuno T, Takeuchi H, Suzumura A. 2015; CCL11 enhances excitotoxic neuronal death by producing reactive oxygen species in microglia. Glia. 63 :2274–2284. [PubMed: 26184677]

Park KW, Baik HH, Jin BK. 2009; IL-13-induced oxidative stress via microglial NADPH oxidase contributes to death of hippocampal neurons in vivo. J Immunol. 183 :4666–4674. [PubMed: 19752235]

Pekny M, Nilsson M. 2005; Astrocyte activation and reactive gliosis. Glia. 50 :427–434. [PubMed: 15846805]

Radu M, Chernoff J. 2013 An in vivo assay to test blood vessel permeability. J Vis Exp. :e50062. [PubMed: 23524912]

Raible DJ, Frey LC, Brooks-Kayal AR. 2014; Effects of JAK2-STAT3 signaling after cerebral insults. JAKSTAT. 3 :e29510. [PubMed: 25105066]

Robbins, SL, Kumar, V, Cotran, RS. Robbins and Cotran Pathologic Basis of Disease. 8. Saunders/Elsevier; Philadelphia, PA: 2010.

Shichita T, Sugiyama Y, Ooboshi H, Sugimori H, Nakagawa R, Takada I, Iwaki T, Okada Y, Iida M, Cua DJ, Iwakura Y, Yoshimura A. 2009; Pivotal role of cerebral interleukin-17-producing gammadeltaT cells in the delayed phase of ischemic brain injury. Nat Med. 15 :946–950. [PubMed: 19648929]

Silver J, Miller JH. 2004; Regeneration beyond the glial scar. Nat Rev Neurosci. 5 :146–156. [PubMed: 14735117]

Skriver EB, Olsen TS. 1986; Edema and atrophy following cerebral stroke. A prospective and consecutive study. Acta Radiol Suppl. 369 :43–45. [PubMed: 2980518]

Skriver EB, Olsen TS, McNair P. 1990; Mass effect and atrophy after stroke. Acta Radiol. 31 :431–438. [PubMed: 2261285]

Smith AJ, Yao X, Dix JA, Jin BJ, Verkman AS. 2017 Test of the ‘glymphatic’ hypothesis demonstrates diffusive and aquaporin-4-independent solute transport in rodent brain parenchyma. elife. :6.

Sui Y, Stehno-Bittel L, Li S, Loganathan R, Dhillon NK, Pinson D, Nath A, Kolson D, Narayan O, Buch S. 2006; CXCL10-induced cell death in neurons: role of calcium dysregulation. Eur J Neurosci. 23 :957–964. [PubMed: 16519660]

Suzuki S, Tanaka K, Nogawa S, Dembo T, Kosakai A, Fukuuchi Y. 2001; Phosphorylation of signal transducer and activator of transcription-3 (Stat3) after focal cerebral ischemia in rats. Exp Neurol. 170 :63–71. [PubMed: 11421584]

Takeuchi H, Jin S, Wang J, Zhang G, Kawanokuchi J, Kuno R, Sonobe Y, Mizuno T, Suzumura A. 2006; Tumor necrosis factor-alpha induces neurotoxicity via glutamate release from hemichannels of activated microglia in an autocrine manner. J Biol Chem. 281 :21362–21368. [PubMed: 16720574]

Thornton P, Pinteaux E, Gibson RM, Allan SM, Rothwell NJ. 2006; Interleukin-1-induced neurotoxicity is mediated by glia and requires caspase activation and free radical release. J Neurochem. 98 :258–266. [PubMed: 16805812]

Topakian R, Barrick TR, Howe FA, Markus HS. 2010; Blood-brain barrier permeability is increased in normal-appearing white matter in patients with lacunar stroke and leucoaraiosis. J Neurol Neurosurg Psychiatry. 81 :192–197. [PubMed: 19710048]

Tzartos JS, Friese MA, Craner MJ, Palace J, Newcombe J, Esiri MM, Fugger L. 2008; Interleukin-17 production in central nervous system-infiltrating T cells and glial cells is associated with active disease in multiple sclerosis. Am J Pathol. 172 :146–155. [PubMed: 18156204]

Vartak DG, Gemeinhart RA. 2007; Matrix metalloproteases: underutilized targets for drug delivery. J Drug Target. 15 :1–20. [PubMed: 17365270]

Waisman A, Hauptmann J, Regen T. 2015; The role of IL-17 in CNS diseases. Acta Neuropathol. 129 :625–637. [PubMed: 25716179]

Wang M, Ding F, Deng S, Guo X, Wang W, Iliff JJ, Nedergaard M. 2017; Focal solute trapping and global glymphatic pathway impairment in a murine model of multiple microinfarcts. J Neurosci. 37 :2870–2877. [PubMed: 28188218]

Wanner IB, Anderson MA, Song B, Levine J, Fernandez A, Gray-Thompson Z, Ao Y, Sofroniew MV. 2013; Glial scar borders are formed by newly proliferated, elongated astrocytes that interact to corral inflammatory and fibrotic cells via STAT3-dependent mechanisms after spinal cord injury. J Neurosci. 33 :12870–12886. [PubMed: 23904622]

Wardlaw JM, Doubal F, Armitage P, Chappell F, Carpenter T, Munoz Maniega S, Farrall A, Sudlow C, Dennis M, Dhillon B. 2009; Lacunar stroke is associated with diffuse blood-brain barrier dysfunction. Ann Neurol. 65 :194–202. [PubMed: 19260033]

Weissberg I, Wood L, Kamintsky L, Vazquez O, Milikovsky DZ, Alexander A, Oppenheim H, Ardizzone C, Becker A, Frigerio F, Vezzani A, Buckwalter MS, Huguenard JR, Friedman A, Kaufer D. 2015; Albumin induces excitatory synaptogenesis through astrocytic TGF-beta/ALK5 signaling in a model of acquired epilepsy following blood-brain barrier dysfunction. Neurobiol Dis. 78 :115–125. [PubMed: 25836421]

Whitehouse PJ, Price DL, Struble RG, Clark AW, Coyle JT, Delon MR. 1982; Alzheimer's disease and senile dementia: loss of neurons in the basal forebrain. Science. 215 :1237–1239. [PubMed: 7058341]

Yang Y, Rosenberg GA. 2011; Blood-brain barrier breakdown in acute and chronic cerebrovascular disease. Stroke. 42 :3323–3328. [PubMed: 21940972]

Yang T, Massa SM, Longo FM. 2006; LAR protein tyrosine phosphatase receptor associates with TrkB and modulates neurotrophic signaling pathways. J Neurobiol. 66 :1420–1436. [PubMed: 17013927]

Yang Y, Estrada EY, Thompson JF, Liu W, Rosenberg GA. 2007; Matrix metalloproteinase-mediated disruption of tight junction proteins in cerebral vessels is reversed by synthetic matrix metalloproteinase inhibitor in focal ischemia in rat. J Cereb Blood Flow Metab. 27 :697–709. [PubMed: 16850029]

Yang T, Knowles JK, Lu Q, Zhang H, Arancio O, Moore LA, Chang T, Wang Q, Andreasson K, Rajadas J, Fuller GG, Xie Y, Massa SM, Longo FM. 2008; Small molecule, non-peptide p75 ligands inhibit Abeta-induced neurodegeneration and synaptic impairment. PLoS One. 3 :e3604. [PubMed: 18978948]

Yang G, Meng Y, Li W, Yong Y, Fan Z, Ding H, Wei Y, Luo J, Ke ZJ. 2011; Neuronal MCP-1 mediates microglia recruitment and neurodegeneration induced by the mild impairment of oxidative metabolism. Brain Pathol. 21 :279–297. [PubMed: 21029241]

Yang T, Massa SM, Tran KC, Simmons DA, Rajadas J, Zeng AY, Jang T, Carsanaro S, Longo FM. 2016; A small molecule TrkB/TrkC neurotrophin receptor co-activator with distinctive effects on neuronal survival and process outgrowth. Neuropharmacology. 110 :343–361. [PubMed: 27334657]

Yu SW, Friedman B, Cheng Q, Lyden PD. 2007; Stroke-evoked angiogenesis results in a transient population of microvessels. J Cereb Blood Flow Metab. 27 :755–763. [PubMed: 16883352]

Zecca L, Youdim MB, Riederer P, Connor JR, Crichton RR. 2004; Iron, brain ageing and neurodegenerative disorders. Nat Rev Neurosci. 5 :863–873. [PubMed: 15496864]

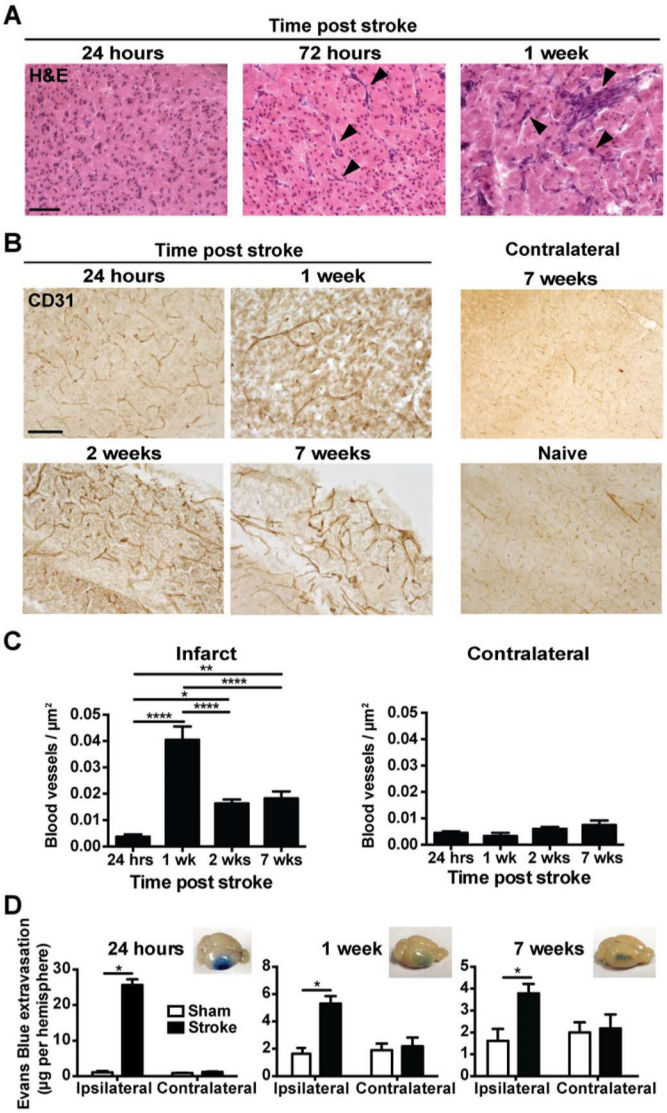

Fig. 1.

Post-stroke angiogenesis results in a population of leaky microvessels. (A) Hematoxylin and eosin (H&E) staining demonstrates that a new network of blood vessels (arrowheads) forms within the infarct during the first week following DH stroke. Scale bar, 100 µm. (B) Anti-CD31 immunostaining demonstrates that the new blood vessels persist within the infarct for at least 7 weeks following stroke. Scale bar, 250 µm. (C) Quantitation of the blood vessel density within the infarct (left graph), as well as in the equivalent area of the somatosensory cortex of the contralateral hemisphere (right graph). Data represent mean ± SEM from n = 4 mice per experimental group. *p < .05, **p < .01, and ****p < .0001 by one-way ANOVA followed by post hoc Tukey's testing. (D) Measurement of Evans Blue extravasation at 24 h, 1 week, and 7 weeks after stroke or sham surgery demonstrates that the blood vessels within the infarct are chronically leaky. Photographic insets show representative images of Evans Blue extravasation. Data represent mean ± SEM from n = 5 mice per experimental group. *p < .05 by Student's *t*-test.

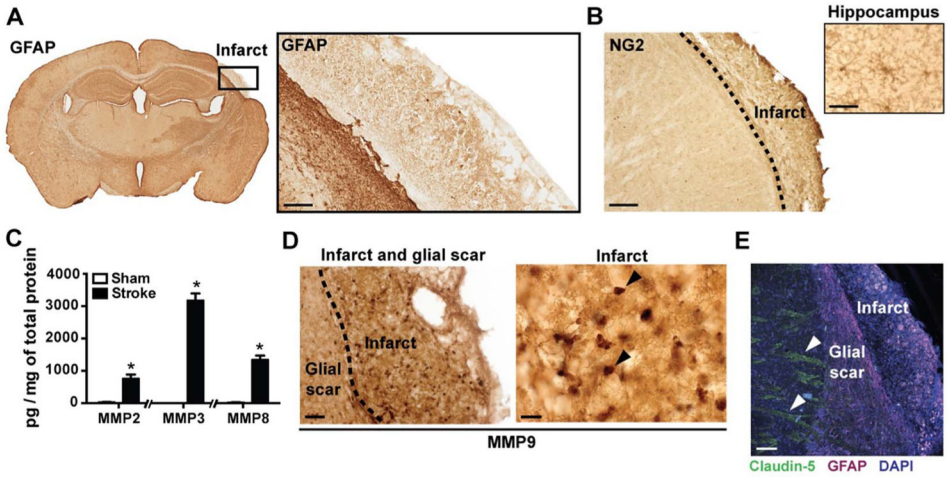

Fig. 2.

Blood vessels within chronic infarcts lack astrocyte support, NG2+ pericytes, and tight junctions. (A) Anti-GFAP immunostaining demonstrates that chronic infarcts are largely devoid of astrocytes. A representative stitched image (from 8 mice) of a brain section (left image) and magnified inset (right image) of GFAP+ immunolabeled astrocytes at 7 weeks post-DH stroke. Scale bar, 100 μm. (B) Anti-NG2 immunostaining demonstrates that chronic infarcts and the glial scar are also devoid of NG2+ pericytes and NG2+ polydendrocytes. Scale bar, 200 μm. The inset is an image of a polydendrocyte taken from the adjacent hippocampus as an antibody positive control. Scale bar, 25 μm. (C) There is a significant increase in expression of MMP2, MMP3, and MMP8 in the area of liquefactive necrosis 7 weeks following stroke compared to the equivalent area in the cortex from sham mice (n = 4 per experimental group). Data represent mean ± SEM. MMPs that are significantly different between stroke and sham mice are denoted in the graphs by asterisks. *$p < .05$ by multiple *t*-tests. (D) Representative images (from 6 mice) demonstrate that there is also increased MMP9 immunoreactivity (arrowheads) in chronic infarcts 7 weeks following stroke (representative of 5 mice). The black dotted line in the left image indicates the location of the glial scar separating the infarct from the surviving tissue. Scale bar, 100 μm for left image; scale bar, 25 μm for right image. (E) There is also a lack of claudin-5 immunofluorescence, a component of tight junctions, within areas of liquefactive necrosis 7 weeks following stroke. A representative image (from 4 mice) is provided showing tight junction protein claudin-5 (green, arrowheads), astrocytes (GFAP, magenta), and nucleic acid marker DAPI (blue) at 7 weeks post-stroke. Scale bar, 100 μm.

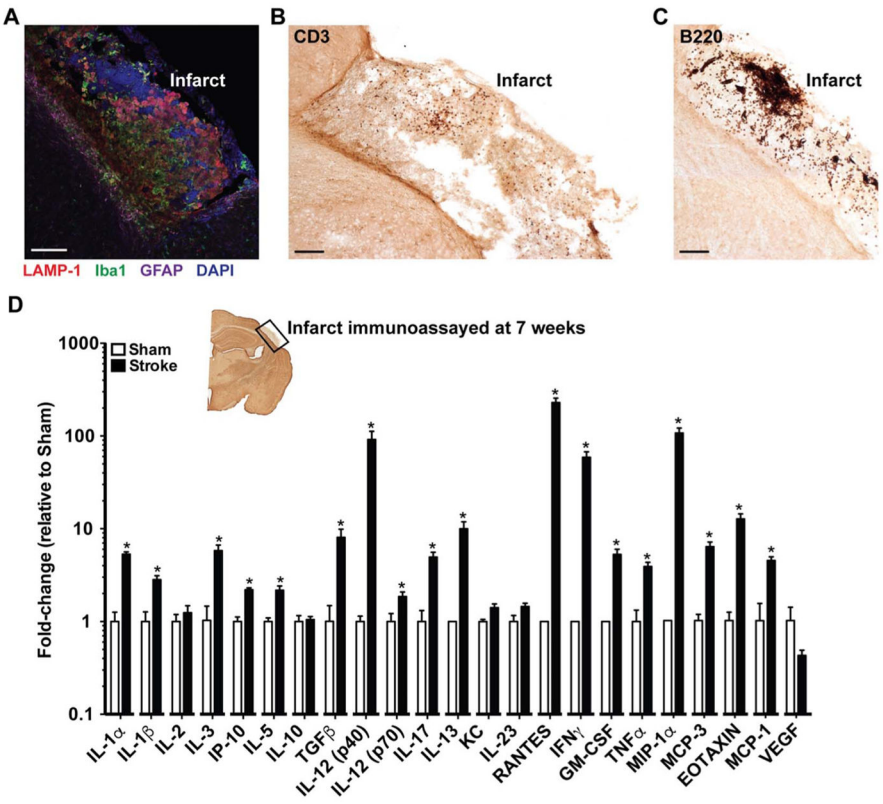

Fig. 3.

Infarcts are sites of chronic inflammation. (A) A representative image (from 5 mice) showing the lysosomal marker LAMP-1 (red), microglia/macrophages (Iba1, green), astrocytes (GFAP, magenta), and the nucleic marker DAPI (blue) reveals substantial LAMP-1 and Iba1 immunoreactivity in a chronic infarct at 7 weeks following DH stroke. (B) A representative image (from 5 mice) revealing abundant CD3+ T-lymphocytes within a chronic infarct at 7 weeks following stroke. (C) A representative image (from 5 mice) revealing abundant B220+ B-lymphocytes within a chronic infarct at 7 weeks following stroke. Scale bar, 100 μm for A–C. (D) Multiplex immunoassays demonstrate that multiple cytokines and chemokines associated with neurotoxicity are present within chronic infarcts (n = 7 mice per stroke group; n = 3 mice per sham group), and are significantly elevated (18 cytokines and chemokines out of 23) in stroke mice compared to sham mice. Data are expressed as a fold-change relative to age matched Sham control values. Data represent mean ± SEM. *p < .05 by Student's *t*-test.

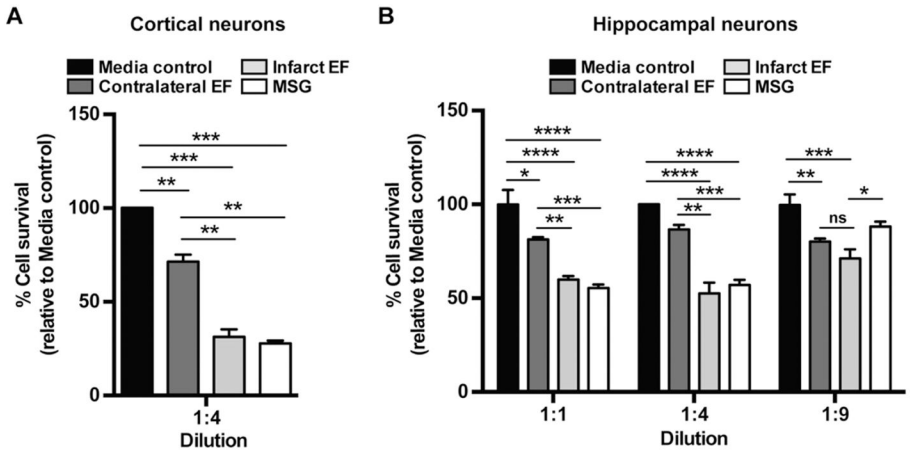

Fig. 4.

Extracellular fluid isolated from the area of liquefactive necrosis is neurotoxic. After allowing primary cortical (A) and hippocampal (B) neurons to mature for 7 days in culture, they were treated with 4 mg/ml extracellular fluid (EF) isolated from either chronic stroke infarcts or the equivalent area on the contralateral hemisphere at indicated dilutions. After 4 h of treatment, neuron survival was determined by the bioluminescent detection of cellular ATP as a measure of viability. Cultures were also treated with 500 μM (for dilution 1:1) monosodium glutamate (MSG) as a positive control. The graph in A shows the combined data from 3 independent experiments (with 3 separate EF sample sets) for dilution 1:4, while the graph in B shows data from 1 experiment for dilutions 1:1 and 1:9, and the combined data from 3 independent experiments (with 3 separate EF sample sets) for dilution 1:4. Data represent mean ± SEM. *$p < .05$, **$p < .01$, ***$p < .001$, and ****$p < .0001$ by one-way ANOVA followed by post hoc Tukey's testing.

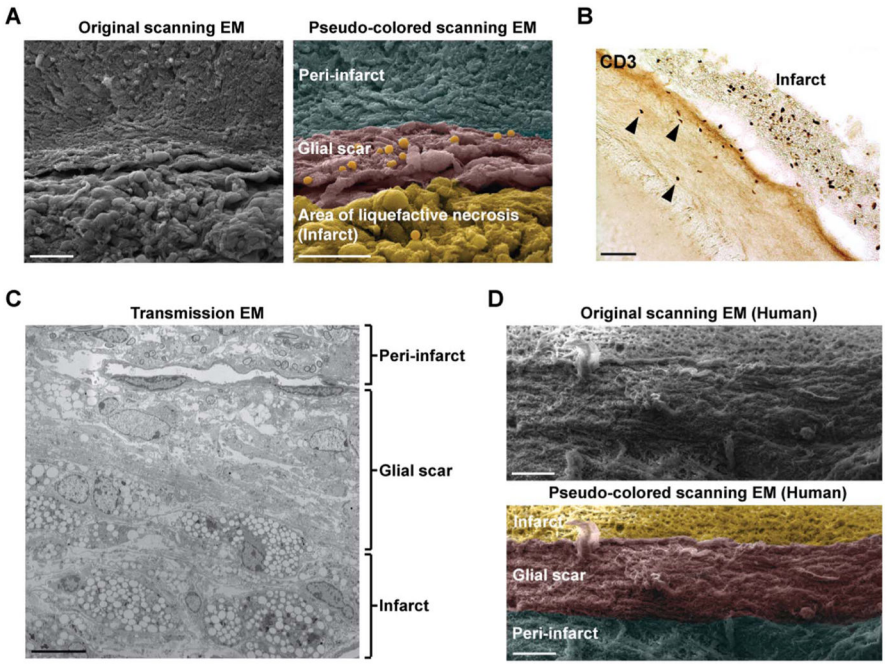

Fig. 5.

The ultrastructure of the glial scar. (A) Scanning EM reveals the ultrastructure of the glial scar at 7 weeks following DH stroke. The glial scar is primarily comprised of hypertrophied astrocytic processes oriented parallel to the area of liquefactive necrosis (representative of 3 mice). Scale bar, 50 μm. Right panel: Higher magnification pseudo-colored version of the same field showing probable lymphocytes (orange) corralled by the glial scar (pink). Scale bar, 25 μm. (B) Anti-CD3 immunostaining suggests that these are T-lymphocytes (representative of 8 mice). Scale bar, 100 μm. (C) Transmission EM reveals that the glial scar is devoid of tight junctions at 7 weeks following stroke (representative of 4 mice). For this analysis, the infarct was identified by the presence of foamy macrophages, the peri-infarct location was identified by the presence of myelinated axons, and the glial scar was identified as the area between these two locations. Scale bar, 10 μm. (D) The ultrastructure of the human glial scar. Top: original scanning EM image. Bottom: pseudo-colored scanning EM image showing the glial scar in pink, the infarct in yellow, and uninfarcted tissue in blue. Scale bar, 150 μm.

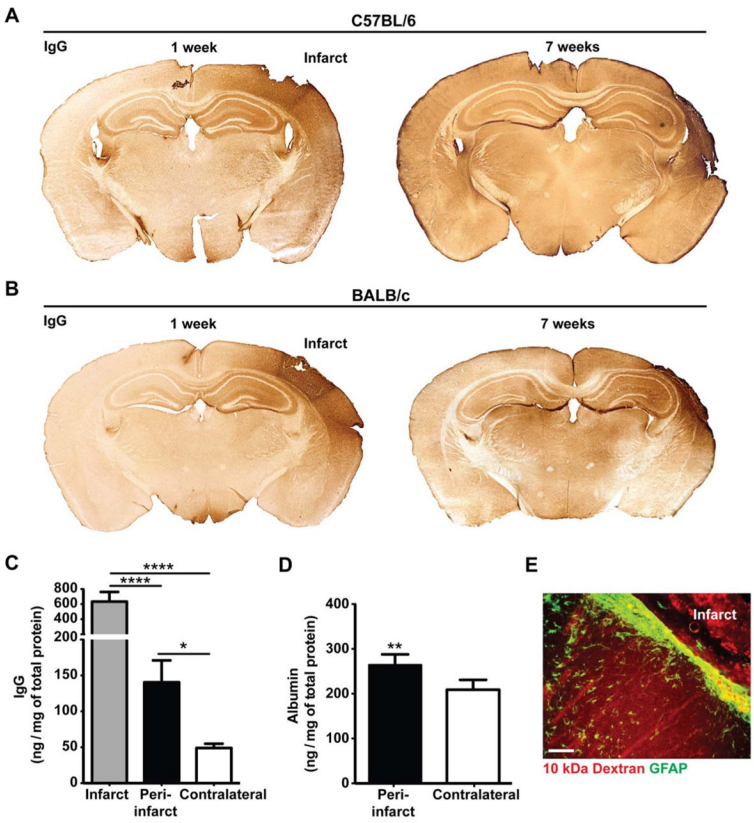

Fig. 6.

Evidence that antibodies and albumin leak across the glial scar and into the brain. (A & B) Representative (from 6 to 8 mice) stitched images of brain sections from (A) C57BL/6 and (B) BALB/c mice immunostained with an IgG antibody to demonstrate that a cloud of antibodies radiates out from the stroke infarct at both 1 week and 7 weeks following DH stroke. (C) IgG concentration by multiplex immunoassay is significantly increased in the ipsilateral hemisphere adjacent to the infarct (peri-infarct) compared to the equivalent area of the contralateral hemisphere at 7 weeks following stroke (n = 20 mice per experimental group). Data represent mean ± SEM. *p < .05, ****p < .0001 by one-way ANOVA followed by post hoc Tukey's testing. (D) Albumin concentration is increased in the area adjacent to the infarct (peri-infarct) compared to an equivalent area of the contralateral hemisphere (n = 20 mice per experimental group). Data represent mean ± SEM. **p < .01 by paired *t*-test. (E) A representative image showing that a 10 kDa Texas Red-labeled dextran injected intraperitoneally into the circulation after 7 weeks post-stroke is found around peri-infarct blood vessels at 6 h following injection. However, it is difficult to discriminate if it has leaked from peri-infarct blood vessels, or from infarct blood vessels and then diffused across the glial scar. Scale bar, 100 μm.

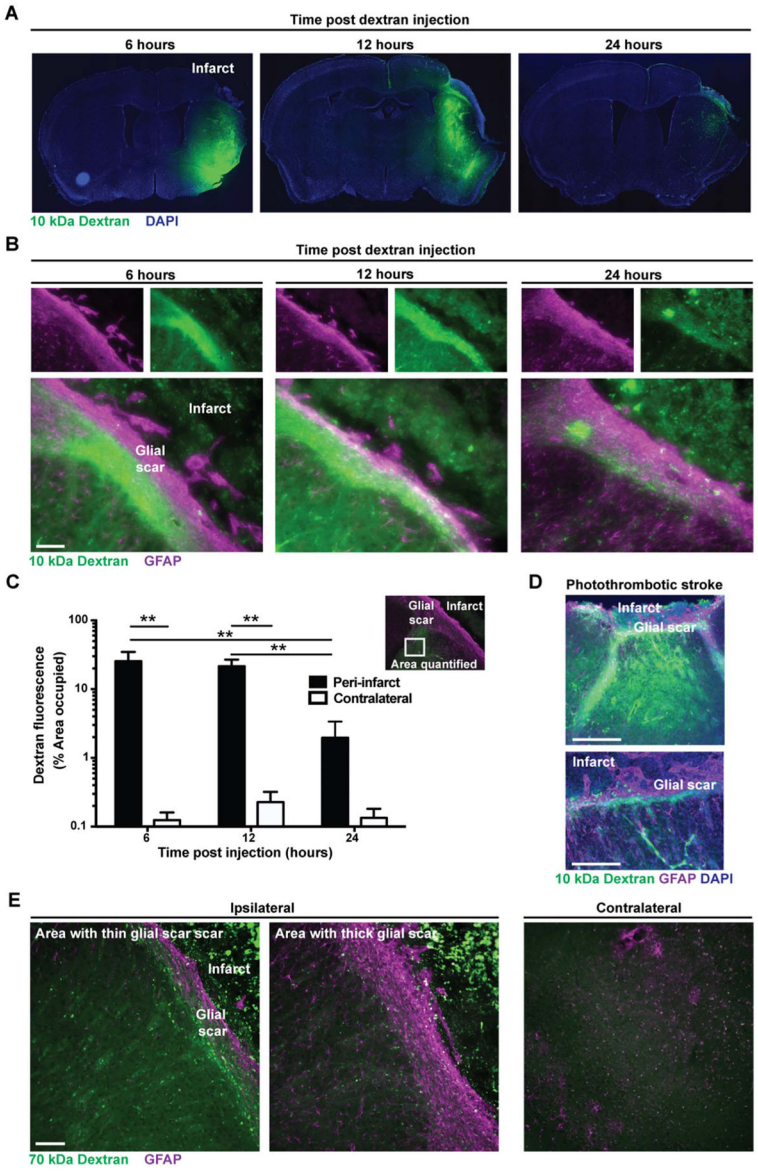

Fig. 7.

Glial scars do not prevent 10 kDa or 70 kDa tracers injected into the area of liquefactive necrosis from leaking into the brain. (A) Representative (from 3 mice per experimental group) fluorescent images of DAPI (blue) stained brain sections from mice injected with a 10 kDa FITC labeled dextran (green) into the area of liquefactive necrosis at 7 weeks following DH stroke. These images reveal a cloud of dextran emanating from the infarct at 6 h (left image) and 12 h (middle image) post-injection, with substantial clearance by 24 h (right image) post-injection. (B) Representative (from 3 mice per experimental group) higher magnification fluorescent images of GFAP (magenta) immunostained brain sections from mice injected with a 10 kDa FITC labeled dextran (green) into the area of liquefactive necrosis at 7 weeks following stroke, and sacrificed at 6 h (left image), 12 h (middle image), and 24 h (right image) post-injection. Scale bar, 100 μm. (C)

Quantitation of significant dextran leakage and clearance in the parenchyma (n = 3 mice per experimental group). Data are expressed as a percentage occupied by dextran fluorescence. Data represent mean ± SEM. **p < .01 by two-way ANOVA followed by post hoc Sidak's testing. (D) Representative fluorescent images of DAPI (blue) and GFAP (magenta) stained brain sections from mice sacrificed 7 weeks following photothrombotic stroke and 12 h post-injection with a 10 kDa FITC labeled dextran (green) into the area of liquefactive necrosis. Bottom image is a higher magnification field from the top image. Scale bars; 1000 μm (top) 250 μm (bottom). (E) Glial scars are permeable to a 70 kDa dextran. Mice were injected into the area of liquefactive necrosis with a 70 kDa FITC labeled dextran (green) at 12 weeks following DH stroke, and euthanized 24 h later. Astrocytes are labeled with GFAP (magenta). Comparison of FITC fluorescence in conjunction with GFAP immunostaining between the ipsilateral and contralateral hemispheres demonstrates that the glial scar is also permeable to molecules 70 kDa in size (representative of 3 mice). Scale bar, 200 μm.

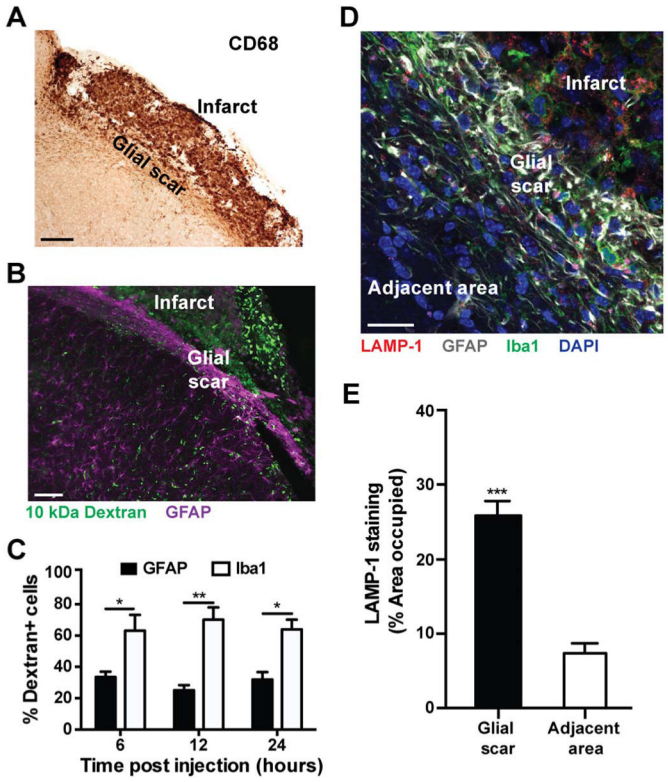

Fig. 8.

Glial scars are endocytic barriers. (A) A representative (from 8 mice) image showing the presence of CD68+ cells within the glial scar at 7 weeks following stroke. Scale bar, 200 μm. (B) Anti-GFAP immunostaining (magenta) of the glial scar at 24 h following injection with the 10 kDa FITC labeled dextran (green) suggests that glial scars are endocytic barriers (a representative image from 3 mice). Scale bar, 200 μm. (C) Quantitation of the colocalization of the 10 kDa FITC labeled dextran with GFAP+ and Iba1+ cells within the glial scar (n = 3 mice per experimental group). Data are expressed as a percentage occupied by dextran + cells. Data represent mean ± SEM. *p < .05 and **p < .01 by two-way ANOVA followed by Sidak's post hoc testing. (D) A representative image showing the lysosomal marker LAMP-1 (red), astrocytes (GFAP, white), microglia/macrophages (Iba1, green), and nuclei marker DAPI (blue) at 7 weeks post-stroke. Scale bar, 50 μm. (E) Quantitation of LAMP-1 demonstrates a significant increase in LAMP-1 expression within the glial scar compared to the adjacent area to the infarct. Data are expressed as a percentage occupied by LAMP-1 staining. Data represent mean ± SEM. ***p < .001 by Student's *t*-test.

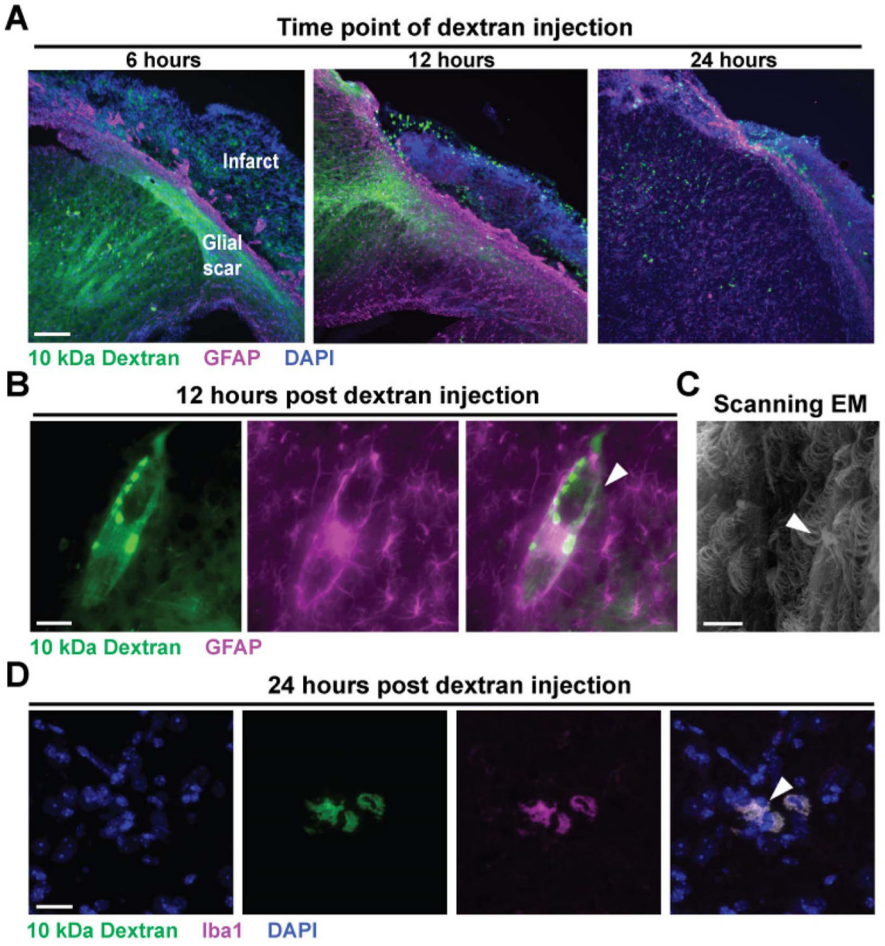

Fig. 9.

Molecules leaking across glial scars are cleared by both microglial endocytosis and paravascular clearance. (A) Representative (from 3 mice per experimental group) low magnification images showing localization of the 10 kDa FITC labeled (green) dextran within the parenchyma at 6 h (left image), 12 h (middle image) and 24 h (right image) following injection after DH stroke. GFAP+ astrocytes are shown in magenta, and the nuclei marker DAPI is seen in blue. Scale bar, 200 μm. (B) A representative (from 9 mice) image showing that the dextran (green) localizes to the paravascular space (arrowhead, right image). GFAP+ astrocytes are shown in magenta. Scale bar, 20 μm. (C) Scanning EM reveals astrocyte complexity, as well as the ultrastructure of an astrocyte surrounding a blood vessel in the parenchyma adjacent to the glial scar (arrowhead) Scale bar, 20 μm. (D) A representative image (from 9 mice) showing that the dextran (green) colocalizes within the parenchyma (arrowhead, right most image) with Iba1+ microglia/macrophages (magenta). Scale bar, 50 μm.

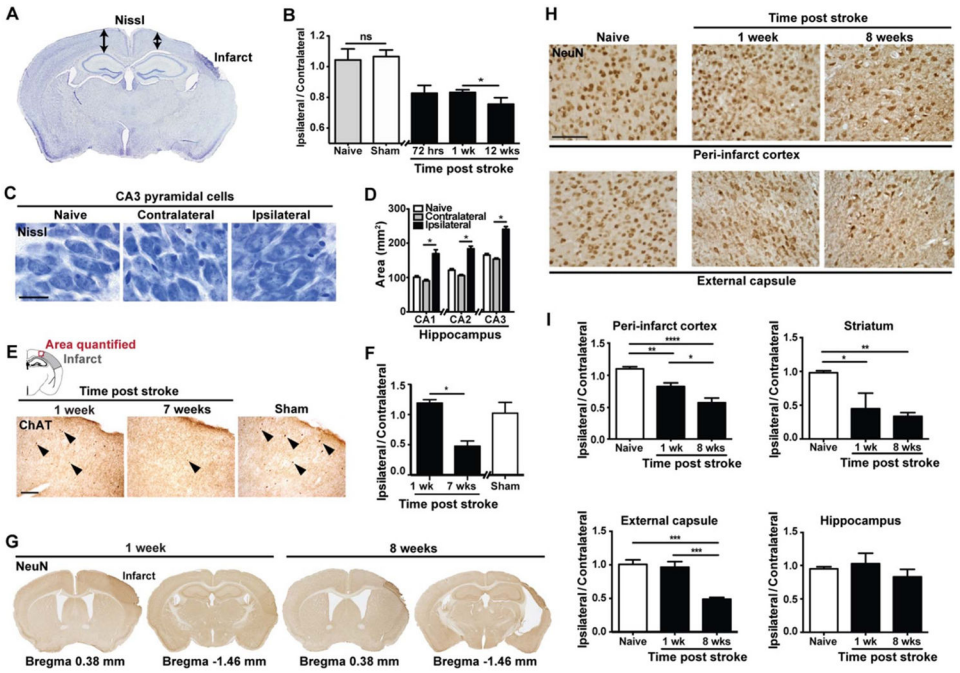

Fig. 10.

Delayed neurodegeneration occurs in regions adjacent to the area of liquefactive necrosis. (A) A representative image of a brain section stained by Nissl at 12 weeks following DH stroke. An area of ipsilateral cortical atrophy is highlighted with double sided arrows in comparison to the contralateral hemisphere. (B) Quantitation of the ipsilateral and contralateral hemispheres demonstrates that atrophy in the form of shrinkage of the ipsilateral hemisphere is significant between 1 week and 12 weeks post-stroke (n = 3–7 mice per experimental group). Data are expressed as the ratio of the ipsilateral versus contralateral hemisphere. Data represent mean ± SEM. Sham mice were sacrificed at 12 weeks following sham surgery. *p < .05 by one-way ANOVA, followed by post hoc Sidak's testing. (C) Representative Nissl images showing cytotoxic edema in CA3 pyramidal cells adjacent to the glial scar in mice at 12 weeks post-stroke compared to CA3 pyramidal cells in the contralateral hemisphere and in naive mice. Scale bar, 25 μm. (D) Measurements of hippocampal regions CA1–3 in Nissl stained brain tissue reveal significant enlargement of the ipsilateral side of the hippocampus (n = 3–7 mice per experimental group). Data is expressed as the area of each hippocampal region. Data represent mean ± SEM. *p < .05 by one-way ANOVA, followed by post hoc Tukey's testing. (E) Representative images of ChAT+ labeled cholinergic neurons (arrowheads) in the ipsilateral cortex from stroke (left and middle images) and sham (right image) mice at 1 week and 7 weeks post-stroke. Scale bar, 200 μm. (F) There is significant loss of ChAT+ neurons in the ipsilateral cortex between 1 week and 7 weeks following stroke (n = 3–7 mice per experimental group). Data are expressed as relative number of ChAT+ neurons or the ratio of ChAT+ neurons in the ipsilateral versus contralateral motor-somatosensory cortex. Data represent mean ± SEM. *p < .05 by Student's *t*-test. (G) Representative images of brain sections immunostained with anti-NeuN at 1 week and 8 weeks following DH stroke. (H) Representative images showing the loss of NeuN immunoreactivity in the peri-infarct cortex and external capsule

in naive C57BL/6 mice and mice at 1 week and 8 weeks post-stroke. Scale bar, 100 μm. (I) Quantitation of NeuN immunoreactivity in the peri-infarct cortex, external capsule, striatum, and hippocampus in the weeks following DH stroke. Data represent mean ± SEM. *p < .05, **p < .01, ***p < .001, and ****p < .0001 by one-way ANOVA, followed by post hoc Tukey's testing.

Table 1

Factors associated with neurotoxicity and neurodegeneration present in areas of liquefactive necrosis.

Factors present in areas of liquefactive necrosis associated with neurotoxicity	Approx. molecular weight (kDa)	Putative mode of neurotoxicity	Selected references
MMP2, MMP3, MMP8, MMP9	72 (MMP2), 54 (MMP3), 65 (MMP8), 92 (MMP9)	Apoptosis induction, blood brain barrier disruption, and demyelination.	(Fujimoto et al., 2008; Mroczko et al., 2013)
Albumin	67	Excitatory synaptogenesis through astrocytic TGF-β signaling leading to epileptogenesis.	(Ivens et al., 2007; Weissberg et al., 2015)
Antibodies	150–900	Antibody-dependent cell-mediated cytotoxicity (ADCC), stimulation of complement, inhibition of signal transduction, and direct induction of apoptosis.	(Ankeny and Popovich, 2010; Doyle and Buckwalter, 2016)
IL-1α, IL-1β	31	IL-1 type 1 receptor activation in astrocytes leads to the production of free radicals and the induction of caspase dependent neuronal death.	(Thornton et al., 2006)
IP-10	10	Treatment of neuronal cultures with exogenous IP-10 produces elevations in intracellular calcium, leading to mitochondrial membrane permeabilization, cytochrome C release, and apoptosis.	(Sui et al., 2006)
IL-17	21	IL-17 can induce cell apoptosis in the CNS in an Act1 and FADD dependent pathway.	(Tzartos et al., 2008; Shichita et al., 2009; Kang et al., 2012; Kang et al., 2013; Waisman et al., 2015)
IL-13	10	IL-13 has been shown to trigger microglial NADPH oxidase-derived oxidative stress, leading to the degeneration of hippocampal neurons in vivo.	(Park et al., 2009)
IFNγ	18	IFNγ receptor can form a neuron-specific, calcium-permeable receptor complex with the AMPA receptor subunit GluR1. Through this receptor complex IFNγ increases calcium influx, decreases ATP production, and leads to neuronal dysfunction.	(Mizuno et al., 2008)
TNFα	17	TNFα can induce excitotoxicity by triggering glutamate release from activated microglia.	(Gelbard et al., 1993; Takeuchi et al., 2006)
Eotaxin	8	Eotaxin can enhance excitotoxic neuronal death by inducing microglial production of reactive oxygen species.	(Parajuli et al., 2015)
MCP-1	13	MCP-1 is an activator of microglial mediated neuronal death.	(Yang et al., 2011)